USE OF A TWO COLOR LIDAR SYSTEM TO STUDY ATMOSPHERIC AEROSOLS

by

Benjamin David Todt

A thesis submitted in partial fulfillment
of the requirements for the degree

of

Master of Science

in

Physics

MONTANA STATE UNIVERSITY
Bozeman, Montana

January, 2010

APPROVAL

of a thesis submitted by

Benjamin David Todt

This thesis has been read by each member of the thesis committee and has been found to be satisfactory regarding content, English usage, format, citations, bibliographic style, and consistency, and is ready for submission to the Division of Graduate Education.

Dr. Kevin S. Repasky

Approved for the Department of Physics

Dr. Richard J. Smith

Approved for the Division of Graduate Education

Dr. Carl A. Fox

STATEMENT OF PERMISSION TO USE

In presenting this thesis in partial fulfullment of the requirements for a master's degree at Montana State University, I agree that the Library shall make it available to borrowers under rules of the Library.

If I have indicated my intention to copyright this thesis by including a copyright notice page, copying is allowable only for scholarly purposes, consistent with "fair use" as prescribed in the U.S. Copyright Law. Requests for permission for extended quotation from or reproduction of this thesis in whole or in parts may be granted only by the copyright holder.

Benjamin David Todt

January, 2010

ACKNOWLEDGEMENTS

I would like to thank Dr. Kevin Repasky for allowing me to work on this project for the last year and a half, and for his guidance in helping me complete this project.

I would also like to thank Tia Sharpe for her help in bringing new instrumentation to the project. Also a thank you to David Hoffman who is responsible for the original design, build, and analysis of the instrument. A special thanks to Erik Carlsten for his invaluable help in making the MATLab programs remarkably faster and more efficient. Also to John Carlsten for his help in writing the final version of my thesis and advisement during my time at Montana State. Finally a thanks to Brent Holben for his efforts in establishing and maintaining the Bozeman AERONET data site.

Funding Acknowledgment

The funding for this project was provided by NASA grant number NNX06AD11G and NASA grant number NNX68AT69A

TABLE OF CONTENTS

TABLE OF CONTENTS – CONTINUED

LIST OF TABLES

LIST OF FIGURES

LIST OF FIGURES – CONTINUED

Figure Page

ABSTRACT

This thesis demonstrates the use of a two color lidar (light detection and ranging) instrument for the purpose of studying atmospheric aerosols. The instrument and the analysis techniques are explained and discussed to provide the necessary background. The calibration is discussed and demonstrated followed by an example of the data analysis. The lidar's combination with a digital camera used to image cloud formations is then discussed and preliminary results are displayed.

INTRODUCTION

This thesis shows the implementation of a two color LIDAR (LIght Detection And Ranging) instrument that is used to identify different aerosol types as well as study their behavior around cumulus cloud formations. For the purpose of studying the effects that cumulus cloud formations have on the aerosol content of the surrounding atmosphere, the two color LIDAR system was combined with a digital camera that takes pictures of the sky at the same time the Lidar system takes data. This system has also been able to work in conjunction with a water vapor DIfferential Absorption Lidar (DIAL) instrument to simultaneously measure optical properties of atmospheric aerosols and water vapor concentrations important for understanding the hygroscopic growth of the aerosols.

Atmospheric Aerosols

In order to come to a better understanding of the global climate it is necessary to have an adequate understanding of atmospheric aerosols. Atmospheric aerosols are capable of changing radiative (atmospheric) forcing both directly and indirectly. Atmospheric forcings are changes in the energy balance of the earth and are measured in the units of heat flux, watts per meter squared $\left(\frac{W}{m^2}\right)$[1][2]. Atmospheric aerosols are capable of causing direct and indirect radiative forcing and are discussed more thoroughly in [1]. The direct effect of aerosols on forcing is based upon the different scattering and absorption of the light by the different species of aerosols. The difficulty in quantifying this effect is that these processes depend on the aerosol species, the location in the atmosphere, and the geographic location where the aerosol is present. For example, the same aerosol located over a snow field compared to a

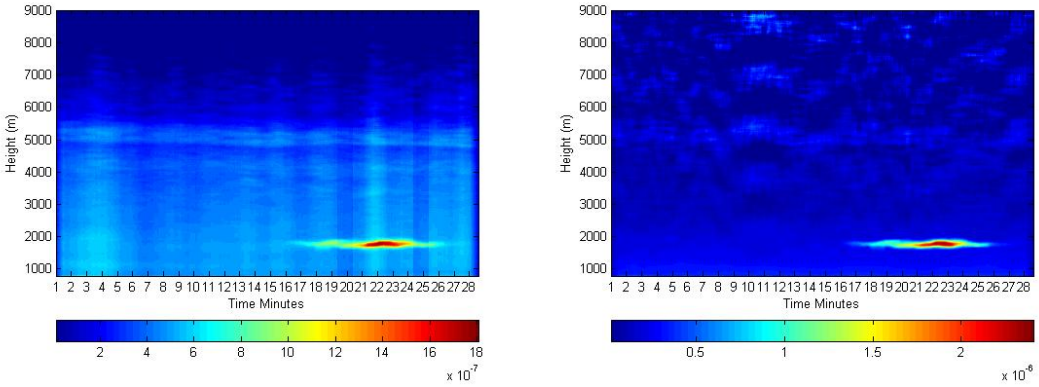

Figure 1: These plots of backscatter show a very short timescale aerosol passing over the instrument, 532 nm is on the left and 1064 nm is on the right.

location over a body of liquid water can have a different effect on the radiative forcing [1]. Compounding this difficulty is that atmospheric aerosols can be present in the atmosphere on vastly different time scales. Figures 1 and 2 demonstrate a short time scale aerosol, while at other times aerosols will occur on longer time scales, hours instead of minutes. Finally the ability to be able to relate radiative forcing to either natural or anthropogenic sources is important for understanding how the climate system is changing.

The indirect effect that aerosols have on radiative forcing can also be large and needs to be more fully understood. When clouds become more reflective they have a negative radiative forcing effect on the climate system. Clouds can become more reflective through the following process. Aerosols increase the cloud condensation nuclei (CCN) concentration. The increase in CCN for a fixed water vapor concentration results in smaller cloud droplet sizes, which reflect more incoming solar radiation. Furthermore, the higher concentration of smaller cloud droplets suppresses drizzle formation affecting the water cycle.

Figure 2: This picture was taken 21 minutes into figure 1 and confirms that it was indeed an aerosol that passed over rather than a cloud.

Because of the wide variability of the effect on radiative forcing based on geographic location, altitude, and aerosol type, the study of effects of aerosols on the climate system must be carried out on a global basis. The aerosol robotic network (AERONET) has been set up to measure column integrated aerosol properties at many different locations around the globe. These studies provide a coordinated effort to measure aerosol properties at various locations using a common sun/sky scanning solar radiometer with a consistent calibration and inversion algorithm. The solar radiometers provide column integrated aerosol properties. Lidar instruments can compliment the solar radiometer data by providing spatial information regarding the aerosol distribution. The results of such data are used to make global climate models more accurate through better modeling of the radiative forcing associated with aerosols.

LIDAR

LIDAR is a technique used to find the distance between a target and the receiver. Laser light is commonly used in LIDAR systems because the spatial, spectral, and temporal characteristics can aid in extracting more information from the light collected by the receiver. The distance to the target is found by measuring the transit time of the light from the source to the target and then back to the reciever as shown in Figure 3. Knowing the transit time and the speed of light in the atmosphere, 3.00×10^8 m/s, allows the distance to the target to be found. The spatial characteristics of laser light are desired because the small divergence associated with the laser beam allows for a precise target area to be illuminated. The characteristic of the spectral distribution of the return signal as well as its temporal component allows for some chemical and physical properties to be inferred. Similarly inferences about the direction and speed of the target can be made by looking at shifts in the spectral component of the return. The powerful part of the LIDAR instrument developed for this thesis project is that it examines two different wavelengths of light and can make inferences about the target atmosphere based upon the relationships of the returns from the two wavelengths. This, when combined with aerosol models allows for the lidar inversion to be completed and the aerosols to be classified.

Lidar Equation

The LIDAR Equation (equation 1) is the critical element of analyzing the returns collected by the lidar receiver. The LIDAR equation takes into account the different factors that have an effect on the light from the time it leaves the transmitter to the

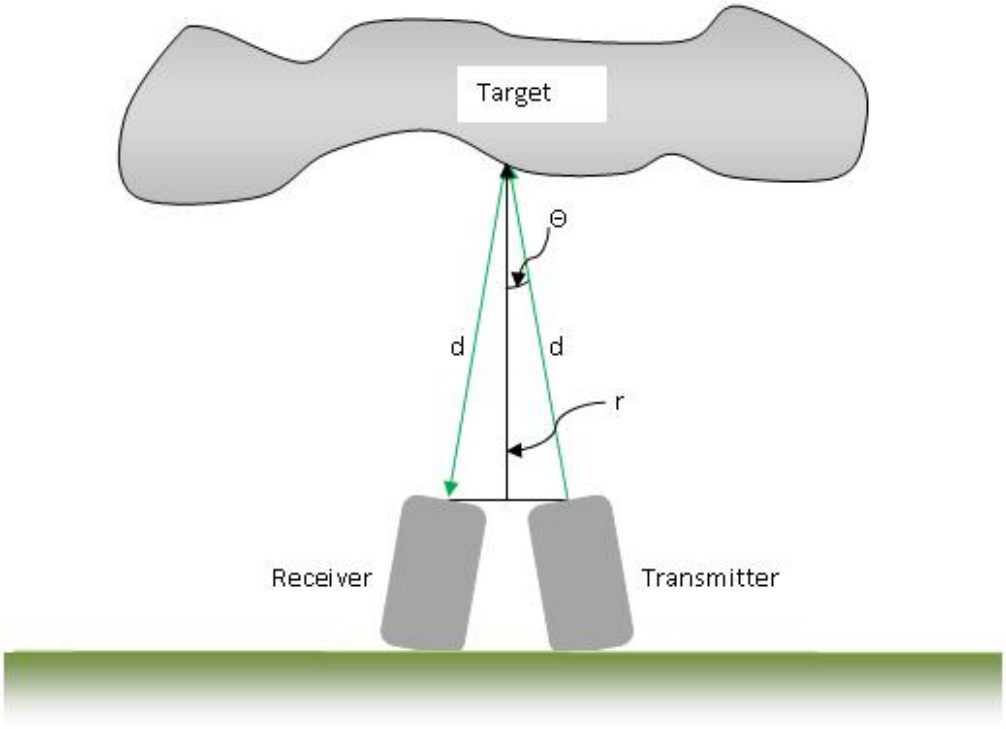

Figure 3: The transit time from the transmitter to the target and back to the reciever is known as t. The range is found by setting it 2d = ct where d is the total distance traveled by the light. With the receiver and the transmitter as close to each other as possible half the distance can be used to find range. $d\cos(\theta) = r$, however because the receiver and transmitter are very close together relative to the range $\cos(\theta)$ is very close to 1 and r can be accurately calculated with $r = \frac{1}{2}ct$.

time it is received by the detector. The lidar equation is

$$P(r) = P_t \frac{A}{r^2} \frac{c\tau}{2} \beta(r) e^{-2\int_0^r \sigma(r')dr'} \epsilon(\lambda)\epsilon(r). \tag{1}$$

In equation 1 P_t is the laser pulse power in Watts from the transmitter, A is the area of the collection optics in m^2, c is the speed of light in m/s, τ is the laser pulse duration in seconds, and $\epsilon(\lambda)$ is the transmission of the receiver optics that is unitless, r is the range in meters. $\beta(r)$ is the backscatter coefficient with units of $(\frac{1}{m \cdot sr})$, $\sigma(r)$ is the extinction coefficient with units of $(\frac{1}{m \cdot sr})$, and $\epsilon(r)$ is the overlap function and is unitless. These are all functions of r because they depend on the range.

In this thesis, the two color lidar developed at Montana State University is described. This thesis is organized as follows. The instrument is described in chapter 2. In chapter 3, the inversion algorithm based on the Constrained Ratio Aerosol Modelfit (CRAM) technique is developed. Calibration of the two color lidar is discussed in chapter 4. Data collected with the two color lidar is presented in chapter 5. Finally, brief concluding remarks are presented in chapter 6.

7

INSTRUMENT

A summary of the design of the two color lidar instrument is described in this chapter. The lidar instrument uses the fundament and frequency doubled outputs of a Nd:YAG laser. Light is collected by a commercial Schmidt-Cassegrain telescope with a photo multiplier tube monitoring the 532 nm return channel and an avalanche photodiode (APD) monitoring the 1064 nm return channel.

Laser Transmitter

The laser transmitter provides the pulsed light that is used to probe the atmospheric aerosols. The laser used is a flashlamp pumped Nd:YAG laser with fundamental 1064 nm and second harmonic 532 nm wavelengths. These wavelengths allow the use of the CRAM technique to be applied to the lidar inversion. This will be further discussed in chapter three. Figure 4 shows a schematic of the transmitter part of the lidar instrument. The Q-switched ND:YAG laser in use produces an approximate 9.9 ns pulse with a power of 50 mJ (100 mJ) for the fundamental (second harmonic) wavelength with a pulse repetition frequency PRF of 20 Hz [2]. The emitted laser beams exit collinearly with a diameter of 0.54 cm. A -2.5 cm focal length divergent lens and a 10 cm focal length convergent lens are used to expand and re-collimate the outgoing laser beam. The beam emerging from the second lens has a diameter of 2.7 cm. The light is then incident on a dielectric mirror that reflects a majority of the 532 nm and 1064 nm light to the atmosphere. The light that is transmitted is incident on a second dielectric mirror which reflects the 1064 nm light and allows the 532 nm to pass through. The reflected 1064 nm light is incident on a pulsed energy monitor. The 532 nm light which passes through the mirror is also incident

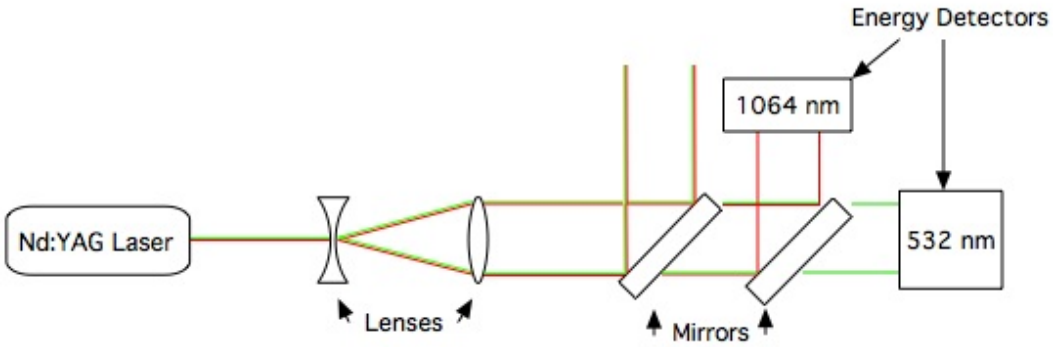

Figure 4: Schematic of the lidar instruments transmitter

on a second pulsed energy monitor [2]. The energy detectors are used to monitor the outgoing pulse energy for each wavelength.

Receiver

The LIDAR receiver collects light scattered in the atmosphere with a 28 cm diameter Schmidt-Cassegrain telescope. At the focus of the telescope is a spatial filter used to reduce the field of view of the telescope to approximately 2 mrad [2]. The divergence angle of the receiver is approximately three times as large as that of the outgoing laser beam eliminating the difficulties involved with the overlap function. The result of the spatial filter controlling the divergence angle is a reduction of the noise on two fronts. First, reducing the area seen by the telescope reduces the amount of ambient light that can reach the detectors and add noise to the signal. Second, reducing the angle seen by the telescope reduces light from the laser that reaches the detectors after undergoing multiple scatterings in the atmosphere.

After passing through the spatial filter the light is collimated and is then incident on a dielectric mirror (figure 5 mirror 1) that reflects the 1064 nm light and passes the

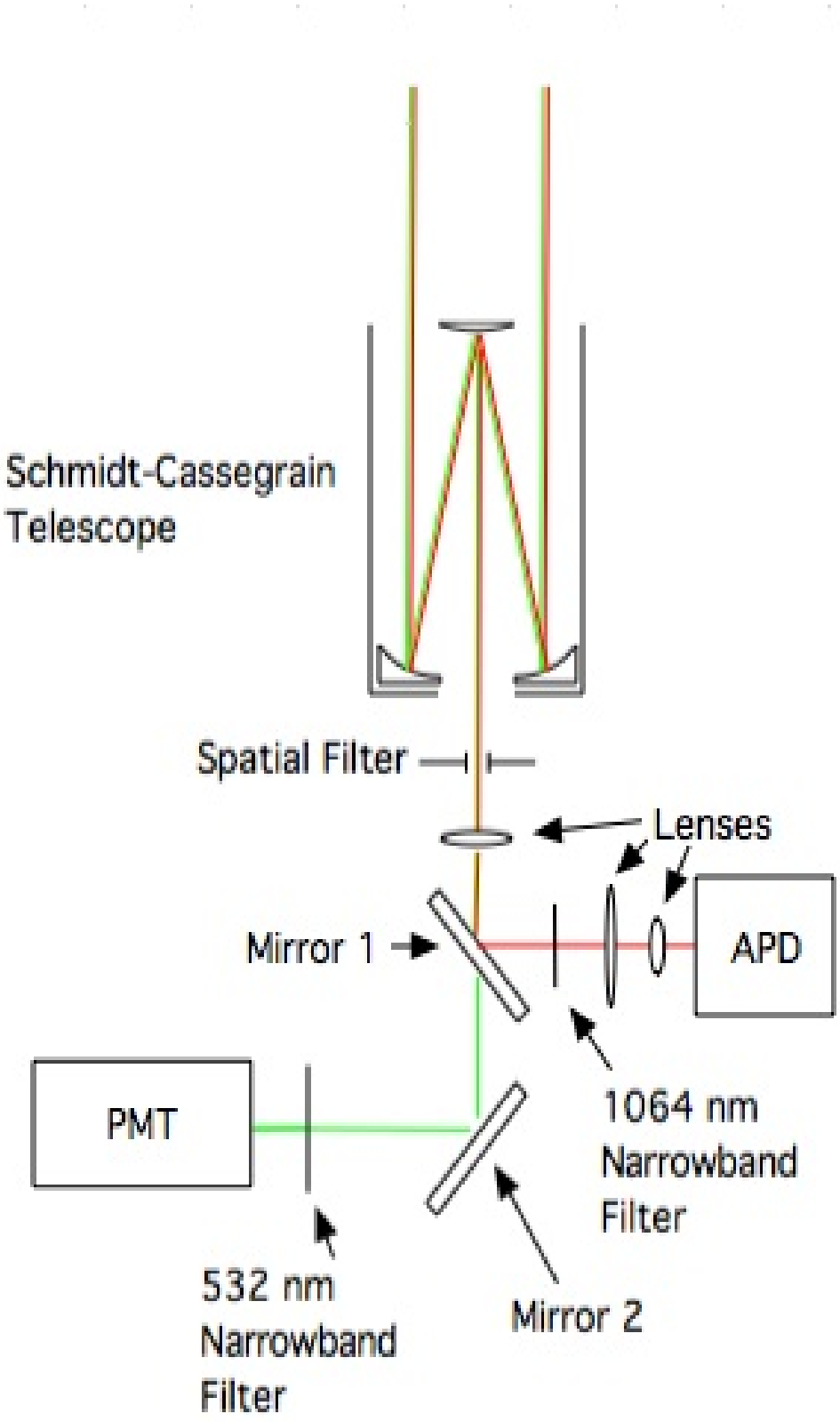

Figure 5: Schematic of the Lidar's receiver

532 nm light. The reflected 1064 nm light is sent through an optical narrow band filter with a 3 nm full width half maximum (FWHM) centered at 1064 nm [2]. The filter ensures that minimal amounts of ambient light are capable of reaching the detector. Lenses of focal lengths 2.5 cm and 0.5 cm are subsequently used to focus the light down onto the 1 mm^2 active area of an avalanche photodiode (APD). The APD is kept in an aluminum light tight box and has a thermoelectric temperature controller which holds the temperature at approximately 5 C during data collection [2]. The 532 nm light that was allowed to pass through the first dielectric mirror is then reflected by a highly reflective mirror (figure 5 mirror 2) onto a 1 nm FWHM narrow band optical filter centered at 532 nm before being collected by a gated photomultiplier tube (PMT).

Limitations set by the data acquisition card in the computer and the amount of noise that still exists in the data means that data from both wavelengths cannot be collected from each pulse by the laser. The data is collected sequentially in the following manner. The first pulse triggers a measurement of the time resolved returns from the 532 nm wavelength by the PMT. Next, the laser's internal shutter is closed and the 532 nm time resolved noise levels are recorded. The shutter is once again opened and the third pulse is measured by the APD which collects the 1064 nm time resolved data. Finally the shutter is once again closed and the 1064 nm time resolved noise is measured. This method is needed for background subtraction because of the time dependent noise introduced by the voltage needed by the Q-switch in the laser transmitter.

Digital Camera

The third component of the system is the digital camera that looks at an area of the sky that includes the laser transmitter's beam. The camera was added to the lidar to provide spatial information regarding clouds. The camera is a uEye UI-1640RE equiped with a Computar Megapixel M1214 lens. The lens has divergence angles 49.2°-40.4°-30.8° D-H-V (diagonal-horizontal-vertical) imaged onto a 1280×1024 $\frac{1}{3}$inch CMOS sensor [3] [4]. The camera is used to view the sky and provide spatial information about the clouds and their position relative to the lidar beam.

The Camera is triggered to take images of the sky by the trigger that comes from the laser and triggers the computer to start taking readings from the PMT and APD. Rather than taking a picture of the sky each time the laser puts out a pulse of light, the trigger is first connected to a circuit which outputs one trigger signal for each four input trigger signals. The result of this is that the camera takes a picture of the sky once for every group of laser pulses that will constitute a single two color profile. This also serves to save memory for the computer.

In order to give the camera an unobstructed view of the sky above the instrument it was not possible to have the camera mounted indoors with the lidar transmitter and receiver. Had this been done the view of the sky would have been obstructed by the roof port. Instead the camera was mounted on the roof near the opening of the roof port. The actual location is displaced approximately three feet laterally and ten feet vertically from the transmitter and receiver of the LIDAR instrument. The wide angle and resolution of the camera cause this to be a negligible distance when viewing atmospheric targets of interest.

The camera was not permanently set up on the roof and therefore needed a mounting system that would be stable, repeatable, and simple. For stability an aluminum

platform was designed and constructed which attached to the edge of the roof port and supported the camera as shown in figure 6. The roof port had the location marked so that the platform could be placed in the same position each time data was taken. A level was also built into the platform to ensure that the platform did not tilt between the many set ups and subsequent take downs. The platform was also designed specifically to have the camera put in only one position so the camera's placement on the platform would not change. Finally, simplicity was desired because the camera was put in place and then taken down each time data was taken this was accomplished by making the mounting mechanism a simple clamp controlled by two easily accessible screws.

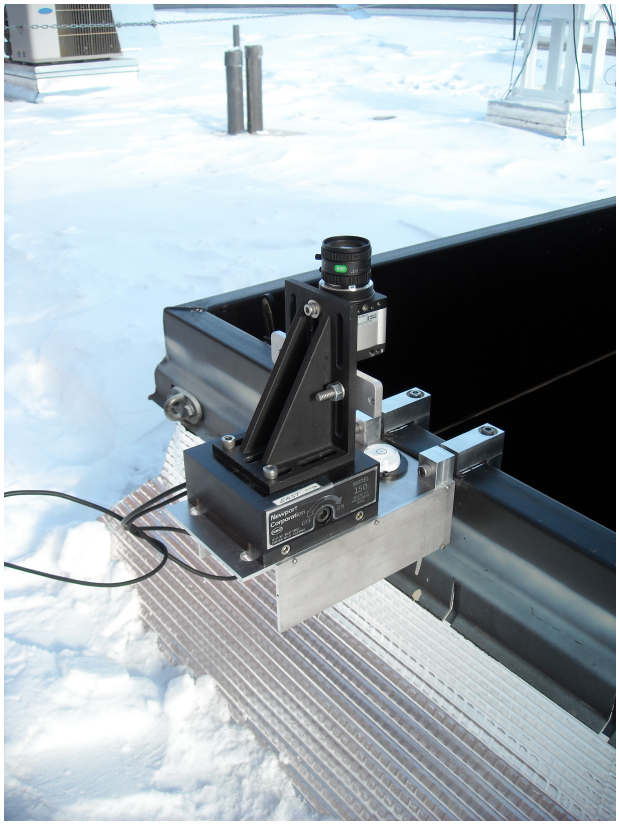

Figure 6: The above picture shows the camera mounted on the roof port in position to take data.

Data Collection

The analog signals from the APD and PMT are collected using a 14 bit analog to digital (A/D) converter operating at 200 MHz [2]. The data recorded after the A/D converter has time dependent noise that results from the high voltage required by the internal Q-switch of the laser. This time dependent noise dictates how the data must be collected. First, the PMT is used to measure the time dependent voltage signal for the 532 nm channel. Next, the laser's internal shutter is closed and the time dependent voltage signal from the PMT for the 532 nm channel is a measure of the time dependent noise. Next, the laser's internal shutter is opened and the APD is used to measure the time dependent voltage signal for the 1064 nm channel. Finally, with the laser's shutter closed a time dependent voltage signal for the 1064 nm channel is collected. The background signal collected with the laser's shutter closed is subtracted from the signal collected with the laser's shutter open for both the 532 nm and 1064 nm channels. This sequence of events is shown in the flow chart shown in figure 7.

The same trigger that is used to trigger the data acquisition card to begin taking voltage measurements from the PMT and APD is also split off and used to trigger the digital camera. The trigger that is split off to the digital camera is sent to a digital circuit that provides only one output pulse for every four input pulses. This synchronizes the camera images with the data taken by the LIDAR. The reason for the one output pulse for every four input pulses is because the laser is triggered four times for each data point.

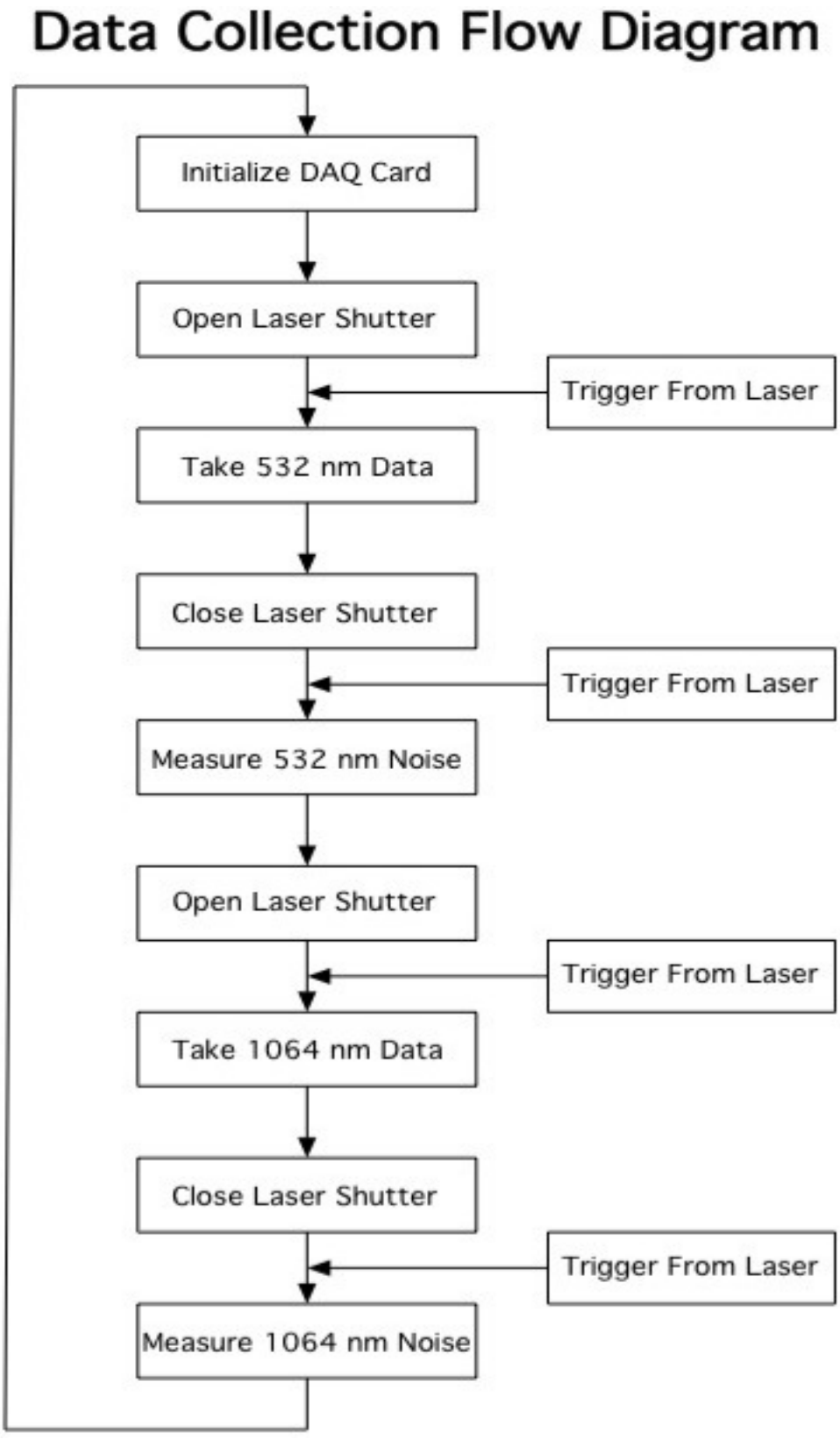

Figure 7: A flow diagram of the data collection as performed by Labview^{TM} software.

THEORY

Lidar Inversion

The lidar inversion for the data collected with the two color lidar is based on methods developed by Fernald et al [5]. Fernald's inversion technique assumes a two component atmosphere with one component leading to Rayliegh scattering from the atmospheric molecules and the second component leading to Mie scattering from the atmospheric aerosols. The lidar equation can be written as

$$P_\lambda(r) = P_{t,\lambda}\frac{A}{r^2}\frac{c\tau}{2}\beta(\lambda,r)e^{-2\int_0^r \sigma(\lambda,r')dr'}\epsilon(\lambda)\epsilon(r) \tag{2}$$

and describes the amount of light received by the detectors from range bin r for a given wavelength λ. In equation 2 $P_{t,\lambda}$ is the power in watts of the laser pulse for each wavelength. A is the are of the collection optics in m^2, c is the speed of light in m/s, τ is the laser pulse duration measured in seconds. The distance to the target or the range is r measured in m. The overlap function is $\epsilon(r)$ whereas $\epsilon(\lambda)$ is the transmission of the receiver optics. The backscatter coefficient is $\beta(r)$ and the extinction coefficient is $\sigma(r)$ measure in units of $\frac{1}{m \cdot sr}$. If all of the constants that are unique to this particular instrument for a particular wavelength are combined into one constant C_λ where

$$C_\lambda = \frac{Ac\tau}{2}\epsilon(\lambda)\epsilon(r) \tag{3}$$

and the round trip atmospheric transmission T^2 is

$$T^2(\lambda,r) = e^{-2\int_0^r \sigma(\lambda,r')dr'} \tag{4}$$

then equation 2 can be written as

$$P_\lambda(r) = \frac{P_{t,\lambda}C_\lambda\beta(\lambda,r)T^2(\lambda,r)}{r^2}. \tag{5}$$

The assumption that the lidar inversion will only be completed when the laser transmitter and the optical receiver are in full overlap allows us to write the overlap function $\epsilon(r) = 1$. Complete overlap for this instrument occurs at 500 meters.

The two component model of the atmosphere takes advantage of the the atmosphere being composed of atmospheric molecules and aerosols. Scattering from atmospheric molecules is described by Rayleigh Scattering. Light scattering from atmospheric aerosols is described by Mie scattering. Separating these two components of the atmosphere allows for the extinction (σ) and the backscatter (β) to be written as

$$\beta(\lambda, r) = \beta_R(\lambda, r) + \beta_A(\lambda, r) \tag{6}$$

$$\sigma(\lambda, r) = \sigma_R(\lambda, r) + \sigma_A(\lambda, r). \tag{7}$$

In equations 6 and 7 β_R and σ_R are the backscatter and extinction associated with Rayleigh scattering from the atmospheric molecules and β_A and σ_A are the backscatter and extinction coefficients associated with Mie scattering from the atmospheric aerosols. The relationship between the aerosol extinction and the aerosol backscatter is written as $S_A(\lambda) = \dfrac{\sigma_A(\lambda, r)}{\beta_A(\lambda, r)}$ and is known as the LIDAR ratio. An equivalent LIDAR ratio can be written for the molecular backscatter and extinction as $S_R(\lambda) = \dfrac{\sigma_R(\lambda, r)}{\beta_R(\lambda, r)}$. The LIDAR ratio is essential to this inversion technique, and is assumed to be constant with altitude. The assumption that the LIDAR ratio remains constant with altitude allows the atmospheric transmission to be written

$$T^2(\lambda, r) = T_A^2(\lambda, r) T_R^2(\lambda, r). \tag{8}$$

It is possible to interpret this to mean that the atmospheric transmission due to aerosols is

$$T_A^2(\lambda, r) = e^{-2S_A(\lambda) \int_0^r \beta_A(\lambda, r')dr'} \tag{9}$$

and that the atmospheric transmission due to molecules is

$$T_R^2(\lambda, r) = e^{-2S_R(\lambda)\int_0^r \beta_R(\lambda, r')dr'}. \tag{10}$$

The molecular backscatter and extinction coefficients associated with the Rayleigh scatter can be modeled. The molecular backscatter is given by

$$\beta_R(\lambda, r) = \frac{374.28\left(\frac{P(h)}{T(h)}\right)}{\lambda^4} \tag{11}$$

where T(h) is the temperature in Kelvin written as a function of height, h in meters, using the lapse rate as

$$T(h) = T_0 - 0.00654h \tag{12}$$

where h is the height above the surface, and T_o is the surface temperature in K. The pressure in Pa is given by

$$P(h) = 1.013 * 10^5 \left(\frac{288.15}{T(h)}\right)^{-5.2199}. \tag{13}$$

Knowing the molecular backscatter allows the molecular extinction to be calculated by realizing $S_R(\lambda) = \frac{8\pi}{3}$.

If the two component atmosphere model is applied to equation 5 and equations 6 and 8 are substituted in the result is

$$P_\lambda(r) = \frac{P_{t,\lambda}C_\lambda[\beta_A(\lambda, r) + \beta_R(\lambda, r)]T_A^2(\lambda, r)T_R^2(\lambda, r)}{r^2} \tag{14}$$

The desired information is found by solving equation 14 for the backscatter coefficient. The technique was described by [5] and is outlined below. If the derivative of equation 9 is taken with respect to the range "r" the result is

$$\beta_A(\lambda, r) = \frac{-1}{2S_A(\lambda)T_A^2(\lambda, r)}\frac{dT_A^2(\lambda, r)}{dr} \tag{15}$$

equation 14 can be substituted into equation 15 resulting in a first order differential equation in T_A^2.

$$\frac{dT_A^2(\lambda,r)}{dr} - 2S_A(\lambda)\beta_R(\lambda,r)T_A^2(\lambda,r) = -\frac{2S_A(\lambda)r^2P_\lambda(r)}{P_{t,\lambda}C_\lambda T_R^2(\lambda,r)} \tag{16}$$

This first order differential equation in T_A^2 can be solved using the standard solution to get the transmission due to the aerosols.

$$\begin{aligned} T_A^2(\lambda,r) = \quad & e^{2S_A(\lambda)\int_0^r \beta_R(\lambda,r')dr'} \times \\ & \left[1 - \frac{2S_A(\lambda)}{C_\lambda}\int_0^r \frac{r'^2P_\lambda(r')}{P_{t,\lambda}T_R^2(\lambda,r')} e^{-2S_A(\lambda)\int_0^{r'} \beta_R(\lambda,r'')dr''} dr'\right] \end{aligned} \tag{17}$$

If a range corrected return is written as

$$L_\lambda(r) = r^2P_\lambda(r) \tag{18}$$

and combined with the substitution of equations 17 and 10 into equation 14 the result is an eqution which solves for the aerosol backscatter.

$$\begin{aligned} \beta_A(\lambda,r) = & -\beta_R(r,\lambda) + \\ & \frac{L_\lambda(r)e^{-2(S_A(\lambda)-S_R(\lambda))\int_0^r \beta_R(\lambda,r')dr'}}{C_\lambda P_{t,\lambda} - 2S_A(\lambda)\int_0^r \frac{L_\lambda(r')}{T_R^2(\lambda,r')} e^{-2S_A(\lambda)\int_0^{r'} \beta_R(\lambda,r'')dr''} dr'} \end{aligned} \tag{19}$$

Because the telescope and the laser pulse are not initially fully overlapped at ranges closer than approximately 500 meters equation 19 must be slightly modified. This is done by having the LIDAR inversion take place over a range from some r_0 to r rather than from 0 to r. If the laser and telescope come into full overlap at r_0 then equation equation 19 is modified to instead be.

$$\beta_A(\lambda,r) = -\beta_R(r,\lambda) + \frac{L_\lambda(r)e^{-2(S_A(\lambda)-S_R(\lambda))\int_{r_0}^{r}\beta_R(\lambda,r')dr'}}{C_\lambda P_{t,\lambda}T^2(r_0) - 2S_A(\lambda)\int_{r_0}^{r}\frac{L_\lambda(r')}{T_R^2(\lambda,r')}e^{-2S_A(\lambda)\int_{r_0}^{r'}\beta_R(\lambda,r'')dr''}dr'} \quad (20)$$

A second change that must be made when considering the inversion from r_0 is that the initial pulse energy must also be scaled. This is simply done by multiplying the initial power $\mathrm{P}_{t,\lambda}$ by $\mathrm{T}^2(\lambda, r_0)$ and setting it as the initial pulse energy.

CRAM

The Constrained Ratio Aerosol Model-fit (CRAM) allows the lidar inversion to be completed by providing S_A at both the 532 nm and 1064 nm wavelengths forming a set of aerosol models [6]. Extensive studies by Cattrall, Reagan, Thome, and Dubovik [7] have produced values for the LIDAR ratio for five distinct different classes of aerosols: Biomass Burning, South East Asia, Urban/Industrial, Oceanic, and Dust. These different aerosol types are the basis for the CRAM which is used by the software to identify aerosols. The LIDAR ratios for each of these particular types are given in table 1. The CRAM model relies on four different relationships in order to identify the aerosols. The first two columns are the LIDAR ratios for different aerosol types followed in parenthesis by the standard deviation, these are used to calculate the backscatter and extinction. The third and fourth columns are ratios of the $\frac{\beta_{550}}{\beta_{1020}}$ and $\frac{\sigma_{550}}{\sigma_{1020}}$ followed by their standard deviations and are used to confirm which aerosols are present. The 550 nm and 1020 nm wavelengths used by the model are different than the wavelengths used by the two color lidar. However, the values are close enough for the relationships and properties described by the model to be accurately applied the data taken by the two color lidar instrument. These numbers were arrived at by

Table 1: Table of values for the Constrained Ration Aerosol Model as found by [7].

Aerosol Species	$S_{A,550}$ (S.D.)*	$\frac{S_{A,550}}{S_{A,1020}}$ (S.D.)*	$\frac{\beta_{A,550}}{\beta_{A,1020}}$ (S.D.)*	$\frac{\sigma_{A,550}}{\sigma_{A,1020}}$ (S.D.)*
Biomass Burning	60 (8)	2.1 (0.3)	1.8 (0.3)	3.8 (0.4)
SE Asia	58 (10)	1.5 (0.3)	1.6 (0.2)	2.4 (0.3)
Urban/Industrial	71 (10)	1.9 (0.3)	1.6 (0.2)	3.3 (0.5)
Oceanic	28 (5)	1.0 (0.2)	1.4 (0.1)	1.5 (0.4)
Dust	42 (4)	1.2 (0.1)	0.9 (0.1)	1.2 (0.1)

*S.D. = standard deviation, Gaussian Distribution

a study of carefully selected AERONET sites. More recent studies of atmospheric aerosols have added further categories to these five in order to be more encompassing.

Utilization of the CRAM model allows for a LIDAR ratio to be chosen to complete the inversion. Using the modeled Rayleigh interaction and an assumed LIDAR ratio the backscatter and extinction coefficients can be calculated. When these values are compared to those given in table 1 it can be determined which type of aerosol is present. If the ratios of $\frac{\beta_{A,550}}{\beta_{A,1020}}$ and $\frac{\sigma_{A,550}}{\sigma_{A,1020}}$ are within one standard deviation of the CRAM value given for the aerosol being tested for the aerosol assumption is deemed to be true. If the values lie outside of one standard deviation then the assumption is deemed to be false.

Instrument Calibration

It is impossible for an improperly calibrated instrument to yield any information of quantitative value. As a result proper calibration is essential for valid inversions of the lidar data to be completed. The calibration of the two different wavelengths must be done differently because of their vastly different interactions with the molecular component of a two component atmosphere.

On very clear days where there are almost no aerosols in the atmosphere, or at higher altitudes where there are very few aerosols, Rayleigh scattering provides the dominant signal. Because Rayleigh scattering can be well modeled it provides an opportunity to calibrate the 532 nm wavelength component of the LIDAR [8]. The range corrected return is given by substituting equation 18 into 14.

$$L_{532}(r) = P_{t,532}\beta_R(532, r)C_{532}T^2(532, r) \tag{21}$$

Equation 21 can be rearranged to solve for C_{532} which is the 532 nm calibration constant. As can be recalled T^2 has the two components, one of which can be modeled for the Rayleigh return, and another part which cannot. In a predominantly Rayleigh scattered return it is assumed that T_A^2 is very close to one, this is confirmed and small adjustments are made to this by using the aerosol optical depth (AOD) taken from a solar radiometer.

The molecular scattering at the 1064 nm wavelength is not strong enough to make a calibration using the same method. Instead the optical depth of high altitude cirrus clouds is used to calculate C_{1064}. Optical depth is a dimensionless parameter that is used to describe the transparency of an object. Equation 22 defines the optical depth τ.

$$I = I_0 e^{-\tau} \tag{22}$$

where I is intensity of the light that passes through the object and I_0 is the intensity of the light immediately before it enters the object.

When looking at the returns from cirrus clouds it is possible to rewrite equation 5 in a new form. First it is helpful to define the range corrected and power normalized return as

$$X(\lambda, r) = \frac{r^2 P(\lambda, r)}{P_{t,\lambda}}. \tag{23}$$

Using equation 23 and rewriting 5 in terms of it we arrive at

$$X(\lambda, r) = C_\lambda \beta(\lambda, r) T^2(\lambda, r). \tag{24}$$

When the assertion is made that only the return from within the cirrus clouds is of interest it is possible to separate the $T^2(\lambda, r)$ into two different terms, one that describes the transition to the bottom of the cloud, $T^2(\lambda, r_{cb})$, and one that describes the transmission through the cloud, $T^2(\lambda, r_c)$.

Taking the ratio of the range and power normalized returns at the 532 nm and 1064 nm wavelengths for $r_{cb} \leq r_c \leq r_{ct}$gives

$$\frac{X(532, r_c)}{X(1064, r_c)} = \frac{C_{532}\beta(532, r_c)T^2(532, r_{cb})T^2(532, r_c)}{C_{1064}\beta(1064, r_c)T^2(1064, r_{cb})T^2(1064, r_c)}. \tag{25}$$

Using the assumption that high altitude cirrus clouds have the same optical depth for the 532 nm and 1064 nm wavelengths, the backscatter and the transmission through the cloud cancel out and the result is.

$$\frac{\int_{r_{cb}}^{r_{ct}} X(532, r_c)}{\int_{r_{cb}}^{r_{ct}} X(1064, r_c)} = \frac{C_{532}T^2(532, r_{cb})}{C_{1064}T^2(1064, r_{cb})}. \tag{26}$$

If equation 26 is rearranged and solved for C_{1064} the result is

$$C_{1064} = \frac{C_{532}T^2(532, r_{cb}) \int_{r_{cb}}^{r_{ct}} X_{1064}(r)dr}{T^2(1064, r_{cb}) \int_{r_{cb}}^{r_{ct}} X_{532}(r)dr}. \tag{27}$$

The property that allows for the equation to be simplified to the form shown in 27 is that high level cirrus clouds have the same optical depth and backscatter at the two different wavelengths [9]. The reason this is the case is that high level cirrus clouds are composed of ice crystals that are much larger than the two wavelengths in question where the geometrical optics limit applies. In that limit both wavelengths have the same backscatter and extinction, and therefore transmission through the cloud. This has been shown in reference [10].

Both of these calibration values were then confirmed using a second. For the 532 nm wavelength the days when the calibration was done were already clear and it was possible to use those same days a second time. The clean continental values for the LIDAR ratios were used to calculate the extinction and the backscatter. It is possible to write the optical depth as a function of the extinction coefficient resulting in

$$\tau = \int_0^r \sigma(\lambda, r')dr'. \tag{28}$$

Like the backscatter and extinction coefficients the optical depth, τ, can also be separated into its molecular and Aerosol components. Applying this change to equation 28 gives

$$\tau_A = \int_0^r \sigma_A(\lambda, r')dr'. \tag{29}$$

Equation 29 shows that using the extinction and integrating it over the entire collected altitude gives the AOD. This value of the AOD was then compared with the value given by the AERONET data. Finding the AOD's to be very similar to each other confirmed that the calibration constants were correct. This procedure was repeated with the 1064 nm wavelength also on clear days.

Confirmation that the calibration constants were indeed correct was not possible until there was a data collected at a time when the aerosol in the atmosphere was well known and abundent. When this occurred there was a layer of smoke over the instrument due to forest fires burning to the west. The analysis clearly showed the smoke to be present and also readily identified the aerosol type as biomass burning. Biomass burning is the aerosol type expected for smoke caused by wildfires.

PROCEDURES

In this chapter the data collection and analysis will be demonstrated. Before the two color lidar can begin taking meaningful data the instrument must first be calibrated. The Calibration of the 532 nm and 1064 nm channels are discussed in this section. With the calibration completed, the data collection and analysis process is discussed.

Sample Calibration

The two color lidar is calibrated so that the data collected can accurately determine information about the atmosphere. Both wavelengths must be calibrated in order for the two color lidar to work properly. The 532 channel calibration is done by comparing the returns from a clear day with the theoretically expected returns from a completely molecular atmosphere. This was discussed in Chapter three and led to equation 21. The molecular scattering for the 1064 nm is a factor of 16 less than the molecular scattering from the 532 nm channel making it difficult for calibration of the 1064 nm channel based on molecular scattering. The 532 nm calibration is used in conjunction with returns from cirrus clouds to find the 1064 nm calibration constant. For these calculations all atmospheric aerosols are assumed to be located below the planetary boundary layer and at altitudes above the planetary boundary layer the atmosphere is modeled using molecular scattering. This assumption is valid on clear days with lower aerosol optical depths.

The 532 nm calibration constant is calculated by averaging

$$C_{532} = \frac{L_{532}(r)}{\beta_{532,R}(r) T^2_{532,R}(r) T^2_{532,A}(r)} \tag{30}$$

over a range where the molecular scattering dominates the return signal. In equation 30, r is the range in meters, the subscripts A and R designate Aerosol and Rayleigh (molecluar) terms respectively, and L is the range corrected return signal. Figure 8 shows a plot of the range and energy normalized returns superimposed upon the expected Rayleigh returns. Figure 9 shows the range and energy as well as Rayleigh normalized returns from the 532 nm channel. The aerosol optical depth was measured to be 0.03 and the calibration constant C_{532} was found to be $1.6017\times10^{7}m^{3}$.

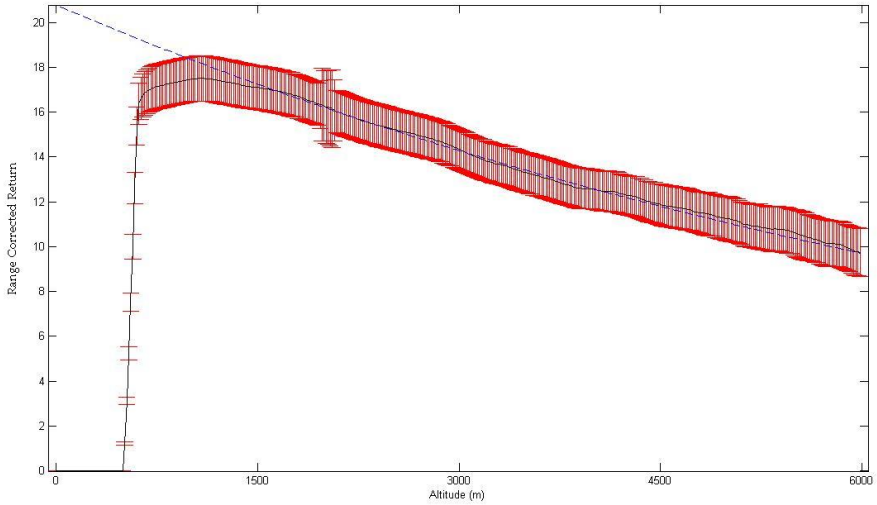

Figure 8: The expected Rayleigh returns (dashed blue line) overlayed with the range and energy normalized returns from the 532 nm channel (solid black line) with error bars (red) showing the confidence in measured points along the normalized return.

A plot of the calculated backscatter based on the calibration constant divided by the modeled molecular backscatter for the 532 nm channel is shown in figure 9. The backscatter was calculated by setting the aerosol backscatter to zero for all r, and the aerosol transmission is set to one in equation 14 and then the equation is solved for β_R. For a well calibrated 532 nm channel, this plot should have a value of one above the planetary boundary layer, above approximately 2 km.

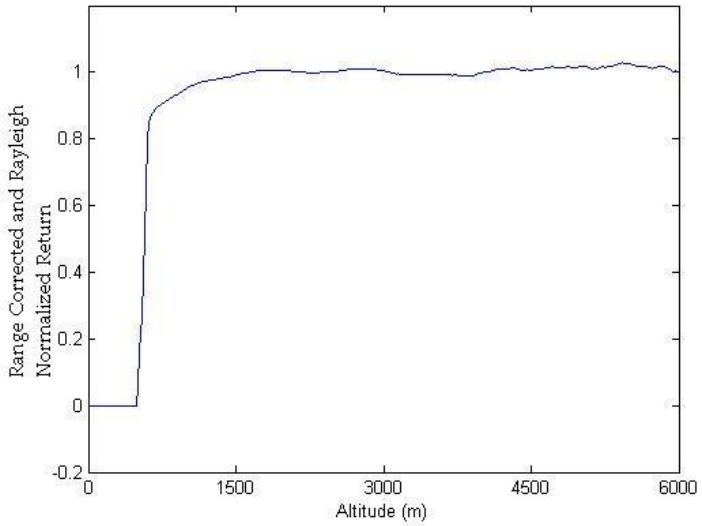

Figure 9: Range, energy, and Rayleigh normalized returns collected by the two color lidar.

Table 2: 532 nm calibration constants determined using molecular scattering method.

Date	Calibration Constant C_{532}
08/12/2008	1.6417×10^7
09/12/2008	1.1228×10^7
09/29/2008	1.2189×10^7
01/09/2009	1.6017×10^7
01/15/2009	1.5446×10^7
01/20/2009	1.6562×10^7

The 532 nm calibration constant was measured on several days when there was a low aerosol optical depth (AOD). Low AOD ensures that the assumption of aerosols being located below the planetary boundary layer is valid. The results of the calibration measurements are shown in table 2. The data from table 2 yields an average calibration constant for the 532 nm channel of 1.4817×10^7 with a standard deviation of 0.2123×10^7 ($\sim$15%).

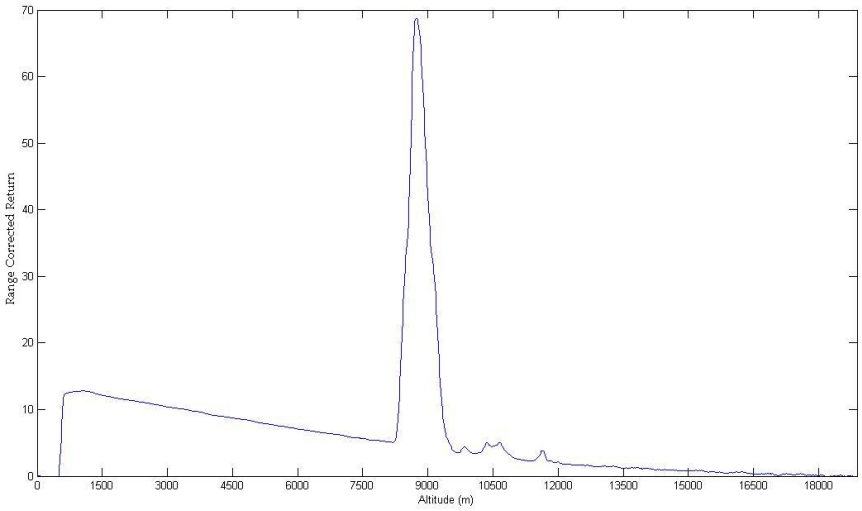

Figure 10: Range corrected return of a cirrus cloud from the 532 nm channel

The 1064 nm channel calibration is done using the relationship shown in equation 31.

$$C_{1064} = \frac{C_{532} T^2(532, r_{cb}) \int_{r_{cb}}^{r_{ct}} X_{1064}(r) dr}{T^2(1064, r_{cb}) \int_{r_{cb}}^{r_{ct}} X_{532}(r) dr}. \tag{31}$$

$T^2_{C,532}$ and $T^2_{C,1064}$ are the round trip transmittances through the cloud and are assumed to be equal. Each return signal is integrated and averaged over the total vertical extent of the cloud to reduce error. Range corrected returns for the 532 nm and 1064 nm channels showing the same cirrus cloud are shown in figures 10 and 11 respectively

The calibration constant for the 1064 nm channel was performed on different days than the calibration of the 532 nm channel because it required high altitude cirrus clouds to be present. The results of the calibration measurements for the 1064 nm channel are sumarized in table 3. This data yields a calibration of the 1064 nm channel of C_{1064} of 1.62×10^6 with a standard deviation of 0.29×10^6 (18%).

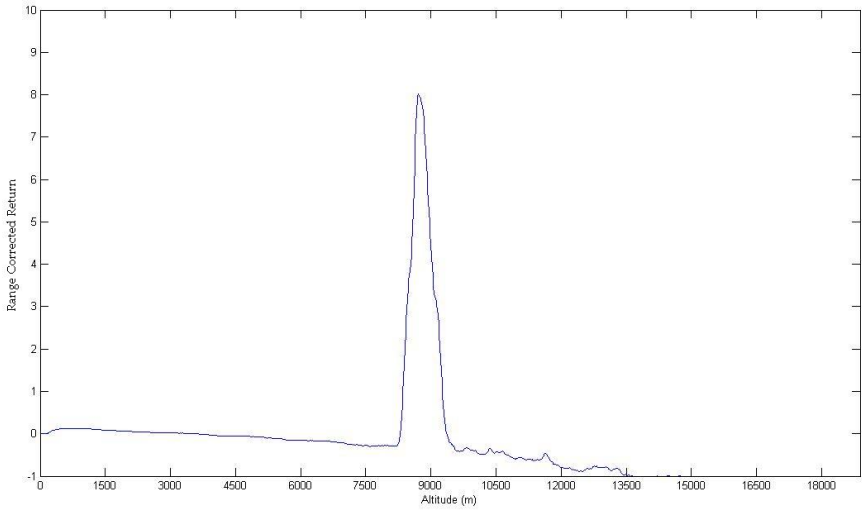

Figure 11: Range corrected return off a cirrus cloud from the 1064 nm channel

Table 3: 1064 nm calibration constant determined using cirrus clouds.

Date	Calibration Constant
01/16/2009	1.28×10^6
01/30/2009	2.06×10^6
02/03/2009	1.67×10^6
02/04/2009	1.79×10^6
02/05/2009	1.33×10^6

Sample Data Analysis.

Data analysis can be completed only after all of the data from a complete run has been taken. The nature of how the data is saved when it is taken causes the data to take up large amounts of space (approximately 2.25 Gb/hr) and take large amounts of time to load into MATLab (approximately 13 minutes to load one hour's worth of data) before it can be evaluated. To expediate this process before any analysis is done the data is loaded into MATLab built into one large matrix and saved as a single file containing all the data. The program that is used to compress the data

is shown in the appendix. While this is a time consuming process it saves countless hours when completing the analysis. The single file is also typically compressed to a size that is two hundred thousand times as small as the original folder.

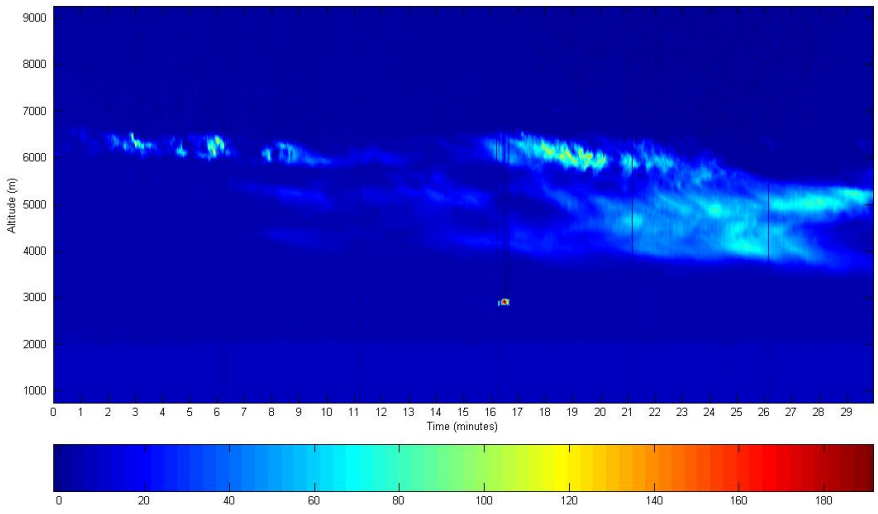

Figure 12: This plot shows the range corrected return for period of data collection on April 20th 2009.

After the data compression has been completed the actual analysis of the data can begin. First the program starts with the raw returns and begins to account for different parameters involved in the inversion that are constants. For example, the power of the lasers output at each wavelength and the sensitivities of the detectors are taken into account. Next the data is scaled by $\frac{1}{r^2}$ in order to give the appropriate range corrected return as seen in figure 12. The range corrected returns are passed to a program which uses the CRAM technique to calculate the backscatter and extinction and test the data for the five different aerosol types and returns the results. The CRAM results are displayed and saved in the format shown in figure 13. If any aerosols are found the parameters for that aerosol type found are used to calculate and save the backscatter and extinction at both the 532 nm and 1064 nm wavelengths.

If none are found then the backscatter and extinction are calculated using a clean atmosphere assumption. When calculating backscatter and extinction coefficients the molecular (Rayleigh) component of the atmosphere needs the temperature and the pressure to be modeled. Temperature being the more varied of these parameters is an input parameter the user controls based on available temperature data from the weather station located very close to the lidar. The temperature data is used in equation 12. The pressure variation is controlled only based upon its relationship with the temperature using equation 13.

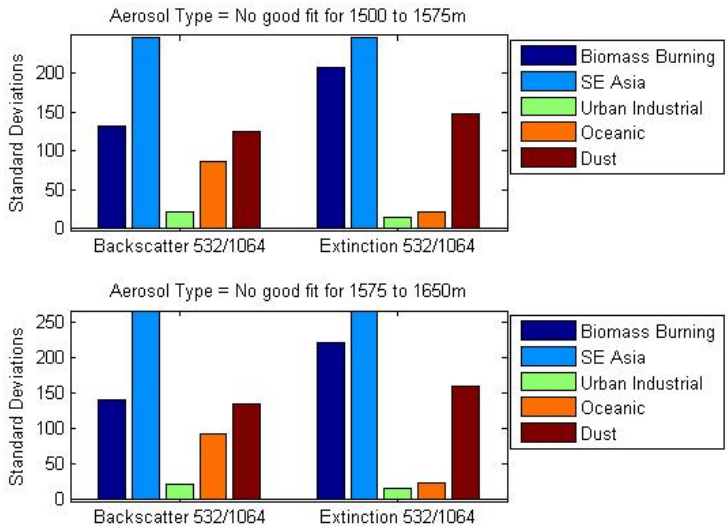

Figure 13: The error measured in standard deviations of the different Constrained Ratio Aerosol Model-fit parameters to the data

In the case shown in figure 13 there were no aerosols identified so the clean, or aerosol free, parameters are used to calculate the backscatter and extinction coefficients.The backscatter and extinction are plotted and saved as figures and saved as matrices. The backscatter at 532 nm corresponding to figure 12 is shown in figure 14. After the backscatter and extinction has been calculated it is possible to use the information to calculate the aerosol optical depth using equation 29. Calculating

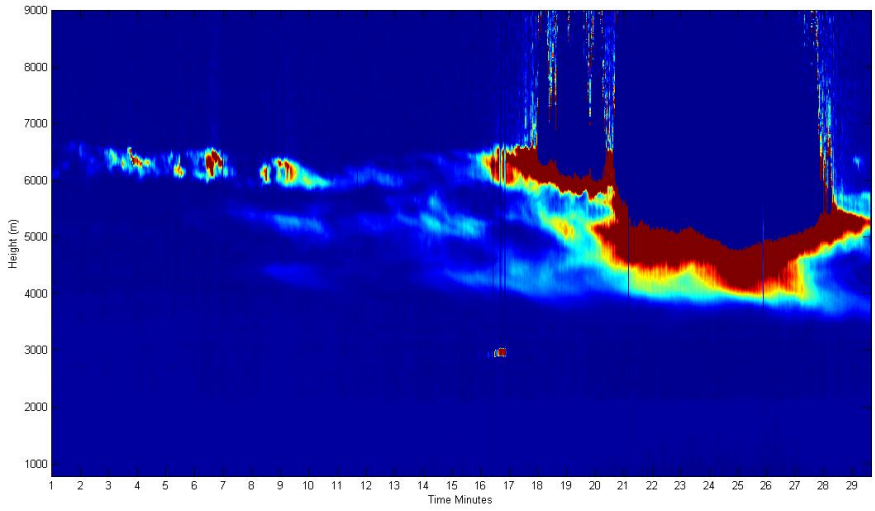

Figure 14: This plot shows the 532 nm backscatter for the same period of data collection on April 20th 2009 as in figure 12.

average AODs at the 532 nm and 1064 nm wavelengths over the first fifteen minutes gave a result of 0.21 for the 532 nm and 0.1 for the 1064 nm channels. The clouds, despite being rather relatively physically thin and appearing optically transparent still have a large effect on the optical depths.

RESULTS

This chapter presents the data collected by the instrument over the time the methods used to create this thesis were developed and used. The CRAM results are shown, and the start of the models expansion for this instrument is explained. Finally the data from the digital camera is combined with the data from the lidar to achieve measurements near the boundaries of cumulus clouds.

CRAM

The CRAM analysis can be well demonstrated with its ability to identify smoke in the atmosphere. The days of September 22nd through the 26th of 2009 the atmospheric conditions above the instrument demonstrated rapid changes between low to high atmospheric aerosol content. On Wednesday the 24th the aerosol optical depth (AOD) above the instrument was approximately .04. Over the course of the night smoke from forest fires moved over the instrument causing the AOD to increase to .15 the following day. On September 25th another drastic change occurred and was captured by the instrument. As can be seen in figure 15 the conditions above the instrument went from being smoke regularly distributed to also having a well defined layer of smoke just below the planetary boundary layer. CRAM analysis displayed in figure 16 shows this layer to clearly be smoke rather than some other type of aerosol. Despite this being previously well known it was further confirmation the model is working properly.

The days of the 22nd and 23rd of September will eventually be used to further expand the CRAM parameters used by the analysis. They will be used to begin to form a category for a continental aerosol model. The cleanliness of the atmosphere

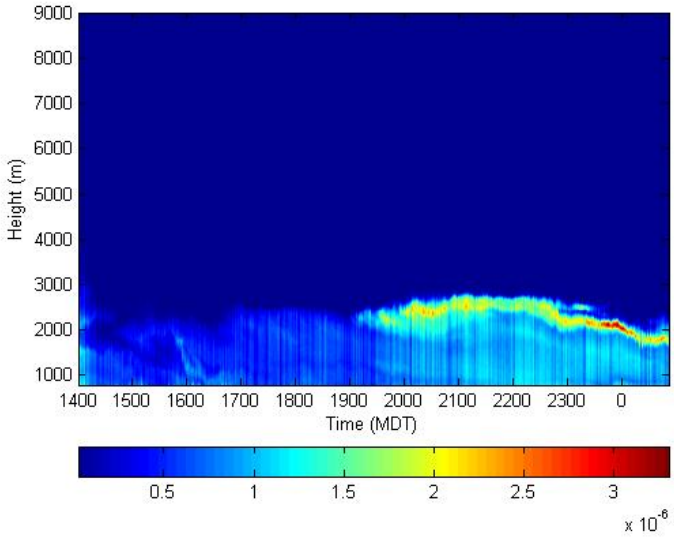

Figure 15: Backscatter at 532 nm clearly shows a layer of smoke starting at about 1900 MDT (Mountain Daylight Time)

was confirmed by the AERONET data available from the AERONET website [11]. Plots of a day with a clean atmosphere (figure 17) and with a smokey atmosphere (figure 18) are shown as examples. While displayed graphically the analytical data is also available on the AERONET website [12]. Unfortunately only having the two days does not give a large number of values off of which to create a statistically valid model. Because there are not yet enough days these two will be kept and had results from other days added to them in order to create a large enough data set to make a statistically valid addition to the CRAM analysis.

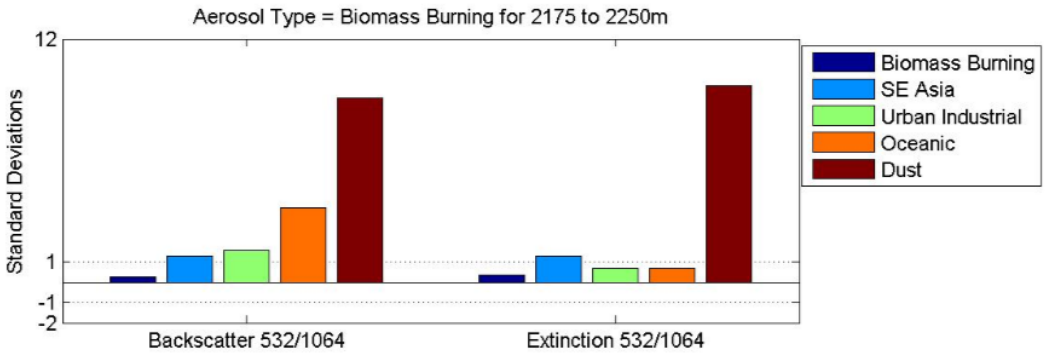

Figure 16: The error for Biomass Burning aerosol type is the only one in which the ratios of $\frac{\beta_{532}}{\beta_{532}}$ and $\frac{\sigma_{532}}{\sigma_{532}}$ are within one standard deviation of the CRAM parameters.

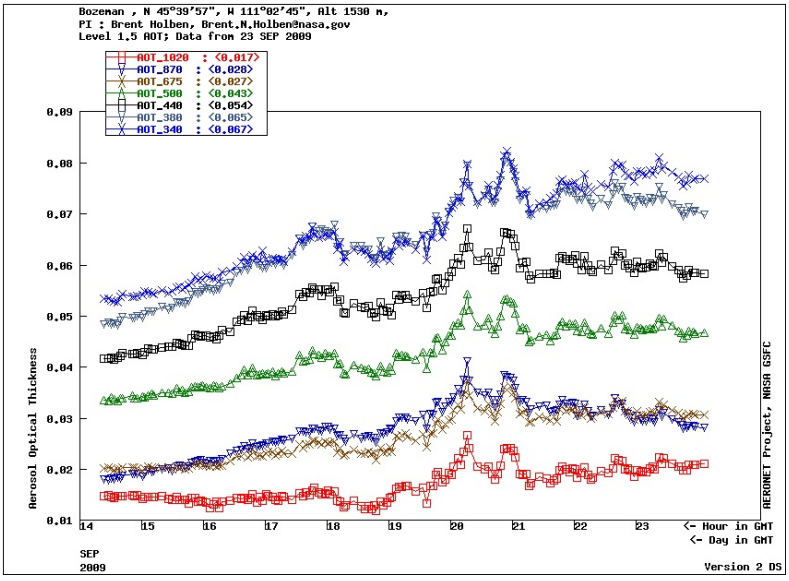

Figure 17: AERONET plot of AOD for a September 23, a day with a low number of atmospheric aerosols [11].

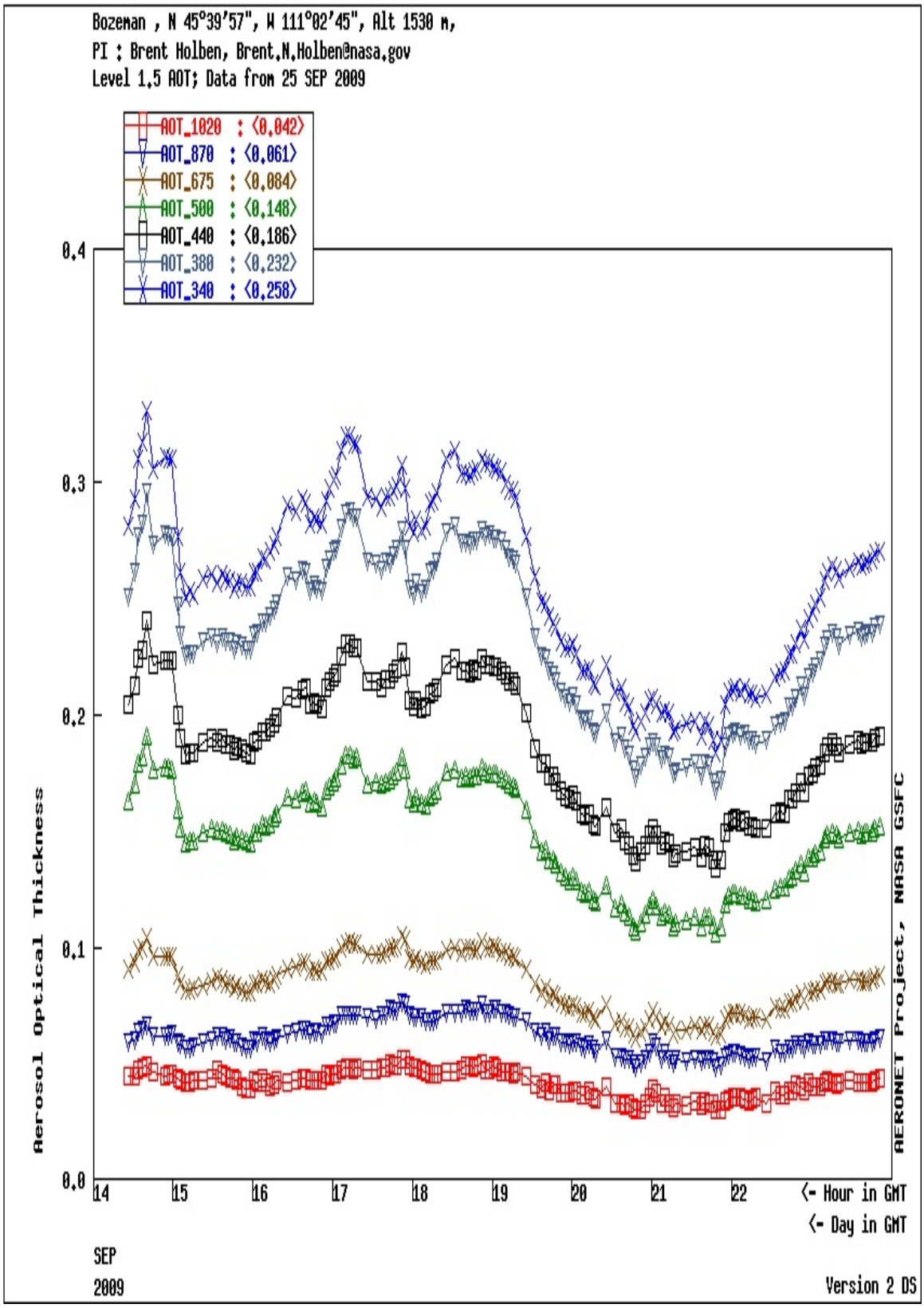

Figure 18: AERONET plot of AOD for a September 25, a day with a higher number of atmospheric aerosols [11].

There are enough days above the instruments location that are very clear and as a result do not fall into any of the catalogued values. As a result, it is desirable to create a new category that specifically describes these clear days above the instrument. Several days have been collected that seem to be good candidates for beginning this sort of classification. A backscatter plot from the 22nd of September which showed very few aerosols in the atmosphere as can be seen in figure 19.

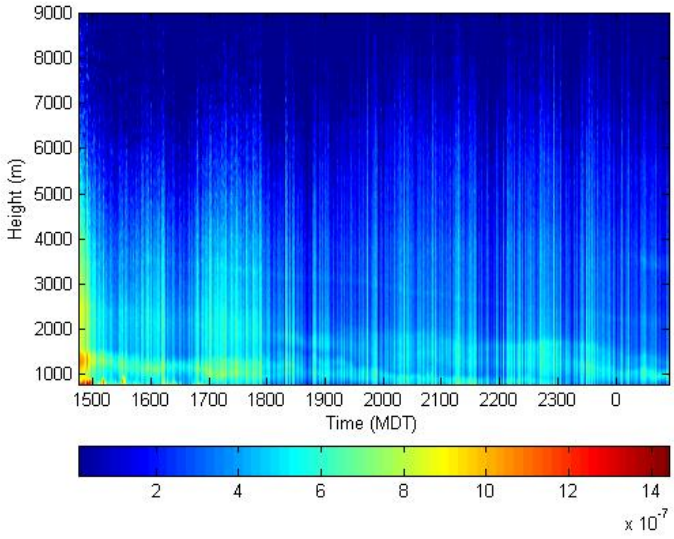

Figure 19: The 532 nm backscatter shows a clean atmosphere

Cloud Boundaries

The combination of the lidar with the digital camera can provide information about how the backscatter and extinction coefficients change near clouds. The transition from cloud to clear sky effects the effective cloud cover important for modeling radiative forcing. The digital camera provides spatial information about the location of the clouds relative to the lidar beam. Measuring changes in the backscatter and extinction as the cloud approaches allows for characteristic tendencies to be measured

and eventually modeled. In order for these measurements to be worthwhile and accurate the cloud must meet several criteria. First the cloud should have well defined boundaries. While at a glance it may seem that many clouds that pass overhead have well defined boundaries this is not the case, and this is especially not the case when they are captured on a digital camera. Second, the cloud needs to move slowly enough across the field of view of the camera. Again while this may not seem to be an issue it does disqualify some clouds. Third the last difficulty is a combination of two different issues. Because of the geographic location of the instrument clouds have a tendency to be in the process of breaking up as they pass over the instrument. The other issue is that the angle of the sun and where in the field of view of the camera the cloud is located can make a clouds appearance vary greatly. The cloud seen in the backscatter of figure (14) shown in the previous chapter is not suitable for several of these reasons. This cloud did not have well defined boundaries as can be seen in figure (20). In figure (20) it is also possible to see that not only were the boundaries not well defined, but the cloud was difficult to distinguish from the higher level cloud cover. This immediately ruled out this cloud because it didn't meet one of the requirements, however, the other two requirements were met by this particular cloud.

A cloud that does meet the requirements and proved useful in these measurements is shown in figure 21. In this cloud it is possible to see reasonably well defined boudaries, no confusion from other clouds, and athough it is not possible to see in a single picture, frame to frame of the movie this cloud was not changing dramatically. When the distance from the cloud vs the backscatter at the level of the cloud are plotted the result is figure 22. As expected it is seen that as the cloud moves away and the distance between the laser and the cloud becomes larger there is a drop in the backscatter at both the 532 nm and 1064 nm wavelengths.

Figure 20: The image shows the cloud that passes over the instrument between minutes 16 and 17.

Because aerosols can have a profound influence on the composition of clouds it is useful to understand these influences. The edges of clouds are one area that needs to be studied in order to properly understand the microphysical interactions taking place. The digital camera's information concerning the spatial information of cloud formations combined with backscatter and extinction information from the lidar can provide this information about this interaction. When the backscatter had been calculated it was examined for areas that were possibly cumulus cloud formations. After these areas had been located the corresponding times on the video were examined to determine whether or not the cloud was suitable.

There were four different cloud formations on two different days that met all the criteria for being able to make measurements. Two clouds on May 4th 2009, and one in June 29th 2009. Figures 22 through 24 show plots of the backscatter as a function of the distance to the cloud. All five of the different plots show an obvious drop in the backscatter as the distance from the cloud increases.

Figure 21: The image shows the cloud passing over the instrument that is useful for measuring the backscatter around the edges.

The plots in figures 22 through 24 make it very easy to see that the backscatter decreases as the distance to the cloud increases. Unfortunately it is difficult to fit a particular regression curve to this data for several reasons. The individuality of each cloud effects both the maximum backscatter within the cloud as well as how quickly the backscatter falls off. Before it will be possible to fit an accurate regression to the cloud data more clouds that have the appropriate characteristics will need to be measured. These five different cloud formations do not form a complete enough data set on which to perform meaningful statistics.

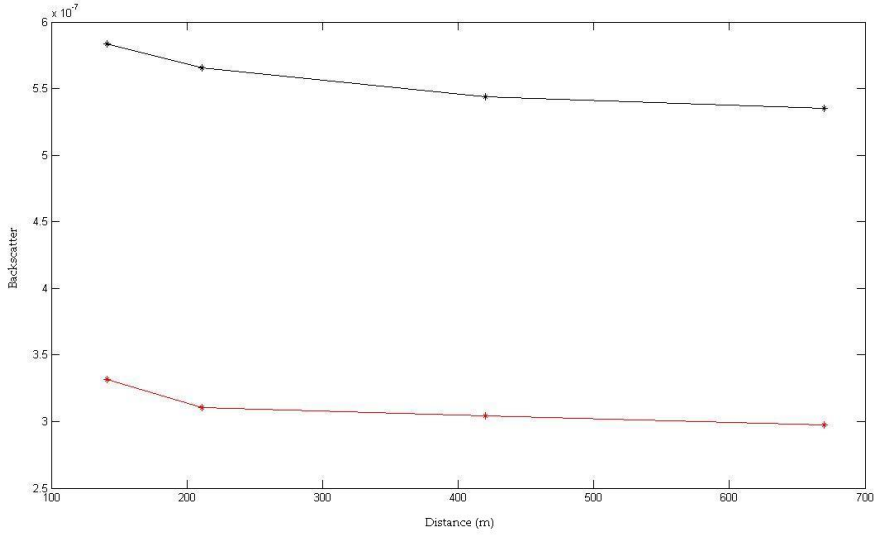

Figure 22: 532 nm (black) and 1064 nm (red) backscatters β plotted as a function of the distance to the cloud for one of the clouds on May 4th 2009.

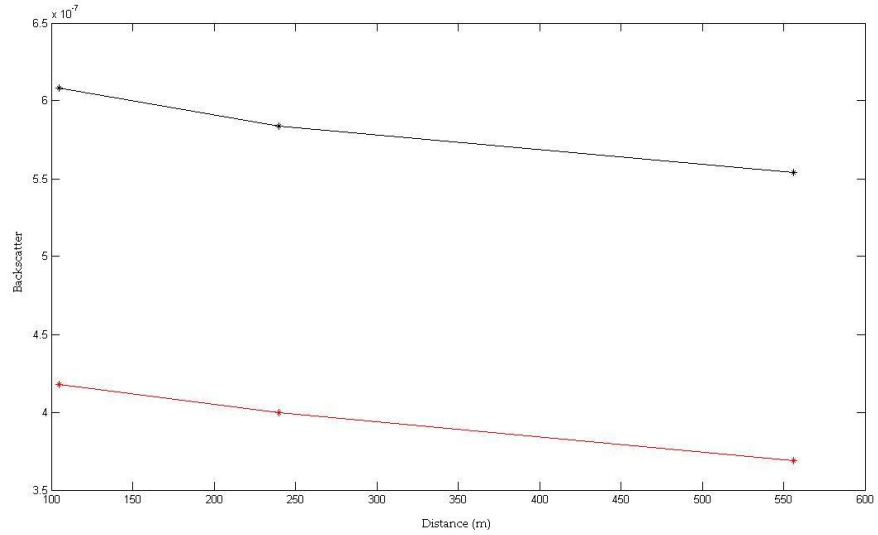

Figure 23: 532 nm (black) and 1064 nm (red) backscatters β plotted as a function of the distance to the cloud for one of the clouds on May 4th 2009.

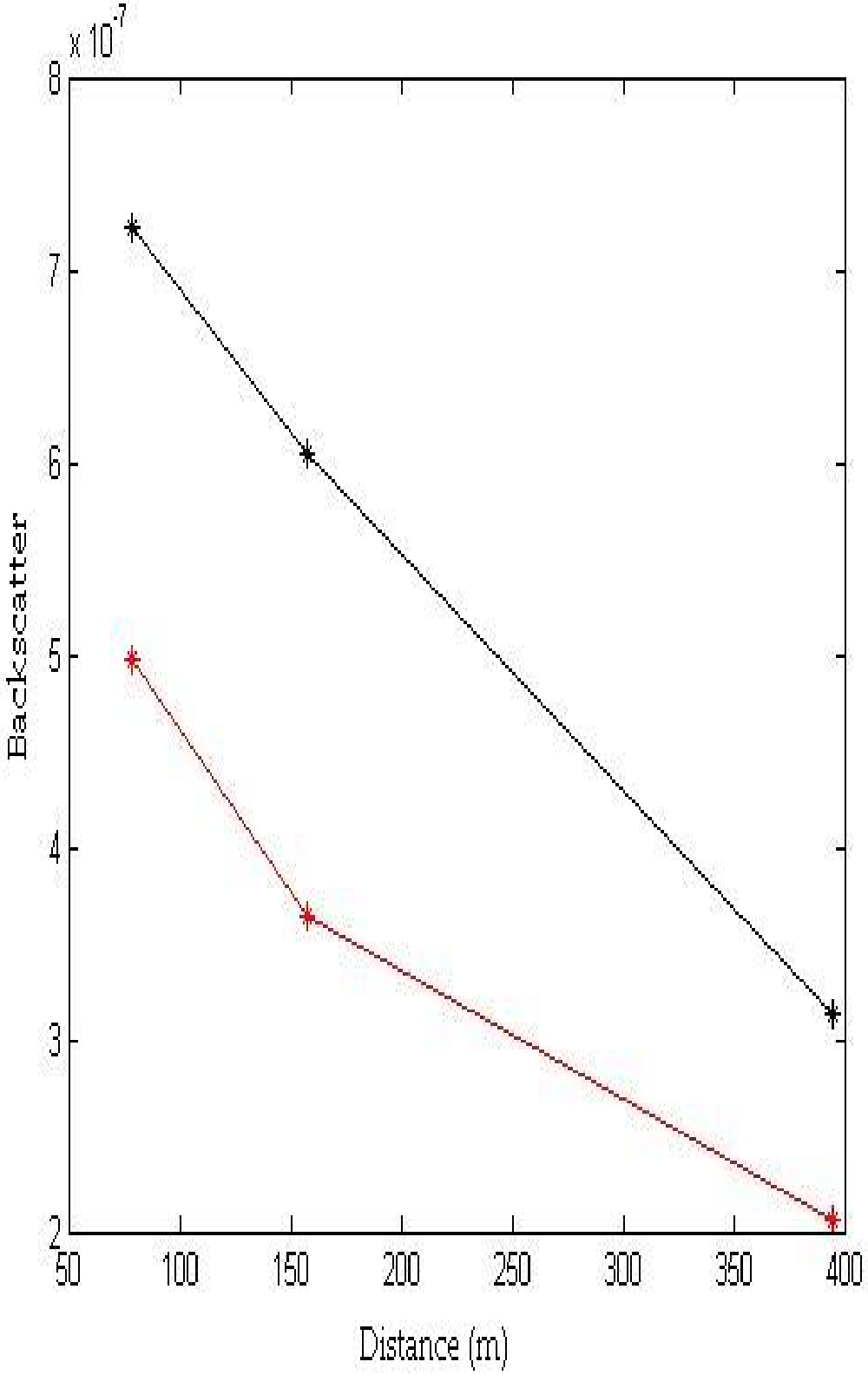

Figure 24: 532 nm (black) and 1064 nm (red) backscatters β plotted as a function of the distance to the cloud for one of the clouds on june 29th 2009.

CONCLUSIONS

The improvements and experiments carried out with the two color lidar instrument over the last year have yielded useful results. It has been possible to make improvements to the instrument and the software while still using them to collect useful data.

The expansions and improvements to the calibration process have allowed for the confidence in them to be increased. The calibration should not be considered complete and should be an ongoing part of the instruments maintenance. The most recent data suggests that the calibration constant has been changing slowly with time. This makes it even more imperative that the calibration constants are calculated and checked on a regular basis to ensure that the data analysis is indeed done accurately.

The studies of clear days have formed a basis for creating a new category within the CRAM analysis used. This category will allow for more days to be categorized and make more complete observations about atmospheric trends. This category needs to be extended further by identifying more days that can be used to characterize it. This will improve its accuracy and usefulness going, although it is already possible to use the category as part of the analysis.

The most important conclusions that can be drawn from this work concern the studies of the areas around cumulus cloud formations. It is possible to see a change in backscatter as the distance to cloud formations changes. However, cloud formations are too diverse in their characteristics to model the interactions of clouds with aerosols off of this alone. Before a meaningful model or fit will be able to be fit to the correlated camera and lidar data many more cloud formations will need to be observed and analyzed. Until the time that this is done it is only possible to conclude that the

backscatter does increase as the distance to cloud formations decreases and that it is possible to measure it with the two instruments currently being used.

FUTURE EXTENSIONS

There are many extensions of this project to be pursued in the future, both in the realm of data analysis and also in furthering the capabilities of the system. Explained below are some areas that are possible extensions of this work. These represent what will need to be a considerable time commitment and effort in order to refine the methods and expand the instruments capabilities.

Analysis Extensions

While the information provided by the AERONET station located on the Montana State University is being used there remain other possible areas where this data could be used. The AOD data provided by the AERONET site is capable of directly making the extinction coefficient data collected more accurate and using it in the CRAM analysis. Unfortunately the AERONET's AOD data is not always available, for example when it is cloudy, or when it is night. Despite this it would constitute a significant improvement with data analysis on the limited extent that it could be used. The improvements that could be made on periods of time when the AERONET AOD data could be used to improve the data analysis procedures even when that data is not available. By creating two independent analysis techniques, one which uses AERONET data and one which doesn't, that produce the same consistent results when all the information was available the one lacking the AERONET should be more reliable because it is found using proven principles from the data when more parameters are available to check against.

Within the current analysis there are also areas where there are possibly better ways to handle the data and as a result make the programs faster, more efficient, and

more user friendly. Ideally analysis should be able to be done with large amounts of user input to allow for different areas of interest to be studied. It would also be useful if a large amount of data could be cataloged for the purpose of finding longer term trends and keeping a permanent record of the localized atmospheric conditions. This process would ideally be something that was as automated as much as possible and required little to no user interaction with the analysis.

It is possible to use the AERONET data to determine the lidar ratios for the 532 nm and 1064 nm channels. Currently this ability is not being used in conjunction with the two color lidar instrument. Calculating the lidar ratios and having them to use as an input would greatly improve the inversion in several ways. Firstly, knowing the lidar ratio makes the CRAM analysis work substantially differently. Rather than using the lidar ratios used by the model and calculating the inversion based on each pair the inversion could simply be calculated once. The CRAM parameters could then be used to compare the final results with. The comparison would allow for the aerosols present to be identified. Calculating the inversion only once rather than five times would substantially improve the speed of the analysis because the inversion is the most time consuming part of the process for the computer. Secondly it would make the data much more quantitatively accurate. Using lidar ratios from the CRAM tables doesn't encompass all the possible lidar ratios, and can in fact correctly identify the aerosol but give values for backscatter and extinction that are slightly off. Using correct lidar ratio would ensure that the backscatter and extinction calculated was indeed accurate and would likely give better results when comparing to the model.

Instrument Changes

In order to make the instrument's setup and operation go more smoothly it would be beneficial to be able to operate the lidar and the digital camera from the same location. This improvement would likely include several different changes. Firstly it would be ideal to have a permanent location and mounting for the digital camera. This would cause there to be an improvement in the stability and repeatability of the camera's placement. Also, a permanent mounting location would need to be encloseable within the roof port room with the instrument which leads to other improvements. With the camera mounted within the room with the lidar it would be possible to keep the computer that records the images in the roof port room as well. This would alleviate the need to take equipment up to the rooftop every time data is going to be taken. Finally, having both computers collecting data in the same place it would be possible for one person to monitor both data collections simultaneously.

Because of the power of the laser used in the lidar it is not eye safe and results in some complications during firing. Because the laser is not eye safe FAA permission is required in order to fire the laser upwards into the atmosphere. Along with the FAA permission, a person is also required to have a view of the sky above the laser at all times when the laser is being fired. The reason for this is to turn off the laser if there is the possibility that an aircraft may be passing over the laser. This has been done by a person sitting on the roof near the roof port for the duration of the data collection time. A significant improvement would be to have another form of interlock that would not require a person to be on the roof. This sort of system may not be possible for any of several reasons, but not requiring a person to be on the roof the entire data collection period would be a significant improvement. Not requiring a person to be located on the roof would be most useful if clearance was obtained to

fire the laser twenty four hours a day. The man hours and inconvenience of location would likely inhibit the ability to fire twenty four hours a day for extended periods of time.

Capability Extensions

As the analysis is improved it would hopefully allow for the system to be used as a tool to study more atmospheric phenomena, especially when the data is studied in conjunction with data from other instruments such as the HSRL, and water vapor DIAL, infrared cloud imager, and higher level AERONET data. While the focus on aerosols as its primary function would stay the same there are still many questions to be answered about how the aerosols interact with other components of the atmosphere and how large of an effect this can be. Collaboration with as many of the aforementioned instruments as possible could begin to answer some of these questions, especially if appropriate time and resources were spent developing the appropriate correlations between the data.

The largest capability extension would be to have the FAA permission to take data twenty four hours a day. During the times when there have been large atmospheric changes occurring it has not always been possible to see them with the instrument because the times when it can be used have been restricted to between 2 pm and 1am local time. The freedom to take data twenty four hours a day would remove many of the restrictions currently on the instrument. For example, atmospheric phenomena like temperature inversions in the are less likely to be observed. Temperature inversions can cause aerosols in the atmosphere to be trapped and concentrated at low altitudes. Their aerosol properties make the two color lidar instrument a useful tool for studying them. Unfortunately where the instrument is located temperature

inversion are likely to form in the morning and revert back to the standard atmosphere by the afternoon. Having the observation time limited greatly reduces the likelihood of observing temperature inversions.

An improvement that could eventually save large amounts of time could be change the program that is used to control the instruments during the data analysis. While LabView does an adequate job during the collection it leaves some things to be desired. It is quite possible that a MATLab program written to control the instruments could provide several benefits. The first benefit would be that the data would be taken and analyzed using the same program. In general MATLab is a faster program than LabView and could allow for some of the data analysis to be started at the same time the data was collected. The main improvement would be that the size of the collected data would be significantly smaller and the compression program would likely not be necessary. The space savings benefit would likely be the most dramatic, it would likely be possible to have the data take less than 2 percent of the space it takes when saved in LabView. Given the rate at which space is taken up 2.25 Gb/hour it takes less than 19 full days of data collection to have one Terabyte of data. Despite storage space being relatively inexpensive it would being able to store at least 50 times the amount of data (more than two and a half years of full day data collection) with the same Terabyte hard drive seems worthwhile. Eliminating the need to compress the data after it has been taken would likely save over ten thousand hours of computer processing time over the two and a half years worth of continuous data collection.

REFERENCES CITED

[1] P. Forster, V. Ramaswamy, P. Artaxo, T. Berntsen, R. Betts, D. Fahey, J. Haywood, J. Lean, D. Lowe, G. Mhhre, J. Nganga, R. Prinn, G. Raga, M. Schulz, , R. V. Dorland. *changes in atmospheric constituents and in radiative forcing.' in: Climate change 2007: The physical science basis. contributions of working group i to the fourth assessment report of the intergovernmental panel on climate change [s. solomon and d. qin and m. manning and z. chen and m. marquis and k.b. averyt and m. tignor and and h.l. miller and eds.].* Cambridge University Press, Cambridge, United Kingdom and New York, NY, USA,, 2007.

[2] David Swick Hoffman. *Two-wavelength lidar instrument for atmospheric aerosol study.* Doctoral Dissertation, Montana State University, April 2008.

[3] Usb ui-1640re. http://www.ids-imaging.com/frontend/products.php?cam_id=45 &sc=1.

[4] M1214-mp. http://computarganz.com/product_view.cfm?product_id=553.

[5] F. G. Fernald, B. M. Herman, J. A. Reagan. Determination of aerosol height distributions by lidar. *Journal of Applied meteorology*, 77:433–448, 1989.

[6] Christopher J. McPherson, John A. Reagan. Analysis of sararan [sic] dust observations by calipso in the context of cram. *Geoscience and Remote Sensing Symposium*, 2:II–570–II–572, 2008.

[7] C. Cattrall, J. Reagan K. Thome, O. Dubovik. Variability of aerosol and spectral lidar and backscatter and extinction ratios of key aerosol types derived from selected aerosol robotic network locations. *J. Geophys. Res.*, 110:433–448, 2005.

[8] John A. Reagan, Christopher J. McPherson, Richard Ferrare, Chris Hostetler, Johnathan Hair. Using combined 532 nm hsrl and 1064 nm elastic-scatter lidar observations to verify and update cram dual-wavelength aerosol retrieval models. *Geoscience and Remote Sensing Symposium*, 2:II–567–II–569, 2008.

[9] J. A. Reagan, X. Wang, M. T. Osborn. Spaceborne lidar calibration from cirrus and molecular backscatter returns. *IEEE Transactions On Geoscience and Remote Sensing*, 10:2285 – 2290, 2002.

[10] Ping Yang, K. N. Liou. Finite-difference time domain method for light scattering by small ice crystals in three-dimensional space. *J. Opt. Soc. Am. A*, 13:2072 – 2085, 1996.

[11] Aeronet data display - site: Bozeman. http://aeronet.gsfc.nasa.gov/cgi-bin/type_one_station_opera_v2_new?site=Bozeman&nachal=2&level=2&place_code=10, October 2009.

[12] Aeronet data download tool. http://aeronet.gsfc.nasa.gov/cgi-bin/webtool_opera_v2_new?stage=3&region=United_States_West&state=Montana&site=Bozeman, October 2009.

APPENDICES

APPENDIX A

MATLAB CODE

Data Compression

```
% fileConverter(dataPath) takes the raw data, and saves it in MATLab
% encoded format. It also averages together 20 rangebins giving the new
% rangebins a size of 15 m.

function [rbins] = fileConverter(dataPath)

tic; % Allows the Operation to be timed.

% This code uses the directory size to automatically find the number of
% files that are available for use in the inversion.

fileData = dir([dataPath '\Bn*']);

maxFileNum = size(fileData, 1) * 2;

% A,An = maxFileNum - 1
% B,Bn = maxFileNum

aMin = 3;
aMax = maxFileNum - 1;
bOffset = 1;

% Loading the first files for A and B allows a the appropriately sized
% matrix to be preallocated.
```

```
A_row = load([dataPath '\A' num2str(aMin) '.dat']) - load([dataPath ...
    '\An' num2str(aMin) '.dat']);
B_row = load([dataPath '\B' num2str(aMin+bOffset) '.dat']) - ...
    load([dataPath '\Bn' num2str(aMin+bOffset) '.dat']);

% rbins is the number of range bins averaged together.
rbins = 20;

% Filtering averages the data, and it is substantially faster than other
% methods of averaging.

filterMask = ones(1,rbins) / rbins;
A_row_filt = filter2(filterMask, A_row);
B_row_filt = filter2(filterMask, B_row);

filtDataRange = (1:rbins:size(A_row, 2));

% Next the Matrices are initialized and then the first row of data is put
% in them.

zeroSize = [( maxFileNum - ( aMin + bOffset ) ) / 2 + 1, ...
size(filtDataRange, 2)];
data_532 = zeros(zeroSize);
data_1064 = data_532;
```

```
data_532(1,:) = A_row_filt(filtDataRange);
data_1064(1,:) = B_row_filt(filtDataRange);

% The for loop gets all of the files and creates a matrix containing all of
% the data for a particular day.

row_i = (aMin+2:2:aMax);

for i = 1:size(row_i, 2)
    try
        A_row = load([dataPath '\A' num2str(row_i(i)) '.dat']) - ...
            load([dataPath '\An' num2str(row_i(i)) '.dat']);
        B_row = load([dataPath '\B' num2str(row_i(i)+bOffset) '.dat']) - ...
            load([dataPath '\Bn' num2str(row_i(i)+bOffset) '.dat']);

        A_row_filt = filter2(filterMask, A_row);
        B_row_filt = filter2(filterMask, B_row);

        data_532(i,:) = A_row_filt(filtDataRange);
        data_1064(i,:) = B_row_filt(filtDataRange);
    catch
        disp(['Check out ' num2str(row_i(i) )]);
    end
end

            % Finally the data is saved
```

```
save([dataPath '\output'], 'data_532', 'data_1064');
toc
```

<u>Calibration</u>

```
function calibration532old(dataPath)
%%%%%%%%%%%%%%%%%%%%%%%%%%%%%%%%%%%%%%%%%
% 532nm Calibration
% Modified 11/13/08 Ben Todt

load([dataPath '\output']);

j = 5000;
top = floor(size(data_532,1) / j) + 1;
dat_532 = [];
dat_1064 = [];
for n = 1:top
    if n > 1
        load([dataPath '\output']);
    end

    % The manipulation program does some quick things to make sure that
    % everything is in the correct format.
    if n  = top
```

```
        data_532 = data_532( (n - 1) * j + 1:n * j,:);
        data_1064 = data_1064( (n - 1) * j + 1:n * j,:);
        [data_532 data_1064 delr] = manipulation(data_532, data_1064, ...
            20);
    else
        data_532 = data_532( (n - 1) * j + 1:size(data_532,1),:);
        data_1064 = data_1064( (n - 1) * j + 1:size(data_1064,1),:);
        [data_532 data_1064 delr] = manipulation(data_532, data_1064, ...
            20);
    end
    dat_532 = [dat_532; data_532];
    dat_1064 = [dat_1064; data_1064];
end

data_532 = dat_532;
data_1064 = dat_1064;

AOD = input('What is the aod? ');
TA532 = exp(-2*AOD); % Optical depth taken from the sun photometer
% These wavelengths aren't exact, use the closest
% ones to it.

delr = 15; % Interval to be used in integration
start = 11;

initial_alt = 1500; % Initial Altitude
```

```
pressure_adjust = -1000; % Adjusted Pressure

L_short1 = mean(data_532,1);

lth = size(L_short1,2) - 1; % Number the size of region of interest
points = 1:lth;
n = start:1:lth+start;
h = n*15 + initial_alt;
T = 288.15 - (.006545.*h);
troposphere = find(h<(21000 - initial_alt));
tropopause = find(h>=(21000 - initial_alt));
T(troposphere) = 288.15 - (.006545.*h(troposphere)); % Temp in Troposphere
T(tropopause) = 216.65; % Temp in Tropopause

% Pressures from Troposphere and Tropopause
p(troposphere) = ((288.15./T(troposphere)).^(-.034164/.006545))...
    .*(1.013e5) + pressure_adjust;
p(tropopause) = exp((-.034164*(h(tropopause) - 11000))/(216.65))...
    .*(2.269e4) + pressure_adjust;

backscatter_M = (374.28*(p./T))./(532^4); % Molecular backscatter
alpha_M = ((backscatter_M .*(8*pi))./3); % Molecular extinction

T2 = h;
for n = 1:lth
    T2(n) = exp(-2*sum(alpha_M(1:n) .* delr));
```

```
end

C532 = (L_short1(points))./(backscatter_M(points) .* T2(points) .* TA532);
%
figure; % Calculation of the 532nm constant for each point
plot(C532); % Plots the constants so that you can see where it is well
% behaved

% Clears unneeded variables

clear TA1064 TA532 points delr start initial_alt pressure_adjust lth n h...
    troposphere tropopause backscatter_M alpha_M T2 T steps row_Matrix ...
    row_Index row_Count p offsetIndex index dir desired_altitude_max ...
    desired_altitude_min day colCount NRG1064

% Messages prompts the user to use the plot to determine the range over
% which to calculate the calibration constant.

message = ('Look at the plot and determine the range of values to');
message = ([message ' take he mean over']);
disp(message);

min = input('Enter the Starting Range Bin '); % Takes User input for the
max = input('Enter the final range bin '); % range over which to
% average
```

```
calibrationConstant = mean(C532(min:max));
disp(calibrationConstant); % Displays calibration constant for 532nm
```

Analysis Drivers

Main Driver Program

```
% This will do the analysis once the initial compression and saving has
% been done.

function smokeLayers2(totalPath, temp)
tic;

for i = 1:1
    % This will load the data and let you know if there is a problem with the
    % path that was entered.

    rbins = 20;

    % This along with the for loop allows for the larger days to be handled as
            % smaller chunks so as to not overstep the cababilities of the computers


    load([totalPath '\output'])
    j = 5000;
    top = floor(size(data_532,1) / j) + 1;
```

```
for n = 1:top
    if n > 1
        load([totalPath '\output']);
    end

    % The manipulation program does some quick things to make sure that
    % everything is in the correct format.
    if n  = top
        data_532 = data_532( (n - 1) * j + 1:n * j,:);
        data_1064 = data_1064( (n - 1) * j + 1:n * j,:);
        [data_532 data_1064 delr] = manipulation(data_532, data_1064, ...
            rbins);
    else
        data_532 = data_532( (n - 1) * j + 1:size(data_532,1),:);
        data_1064 = data_1064( (n - 1) * j + 1:size(data_1064,1),:);
        [data_532 data_1064 delr] = manipulation(data_532, data_1064, ...
            rbins);
    end

    % The first user input asks for the temperature so that the atmospheric
    % conditions can be accurately modeled

    userTemp = 273.15 + temp;

    [beta_532 beta_1064 sigma_532 sigma_1064] = betaSigmaDriverNewer(...
```

```
    data_532, data_1064, delr, userTemp, i);

    save([totalPath '\beta5mat' num2str(n)], 'beta_532');
    save([totalPath '\beta10mat' num2str(n)], 'beta_1064');
    save([totalPath '\sigma5mat' num2str(n)], 'sigma_532');
    save([totalPath '\sigma10mat' num2str(n)], 'sigma_1064');
end

beta_532Total = [];

for m = 1:top
    load([totalPath '\beta5mat' num2str(m)]);
    beta_532Total = [beta_532Total; beta_532];
end

save([totalPath '\beta_532Totalforplot'], 'beta_532Total');
clear beta_532Total

beta_1064Total = [];

for m = 1:top
    load([totalPath '\beta10mat' num2str(m)]);
    beta_1064Total = [beta_1064Total; beta_1064];
end

sigma_532Total = [];
```

```
    save([totalPath '\beta_1064Totalforplot'], 'beta_1064Total');
    clear beta_1064Total

    sigma_532Total = [];

    for m = 1:top
        load([totalPath '\sigma5mat' num2str(m)]);
        sigma_532Total = [sigma_532Total; sigma_532];
    end

    save([totalPath '\sigma_532Totalforplot'], 'sigma_532Total');
    clear sigma_532Total

    sigma_1064Total = [];

    for m = 1:top
        load([totalPath '\sigma10mat' num2str(m)]);
        sigma_1064Total = [sigma_1064Total; sigma_1064];
    end

    save([totalPath '\sigma_1064Totalforplot'], 'sigma_1064Total');
    clear sigma_1064Total
end
```

Driver for Backscatter and Extinction Calculations

```
% This function will drive the calculation of the backscatter and
% extinction.

function [beta_532 beta_1064 sigma_532 sigma_1064] = ...
    betaSigmaDriverNewer(data_532, data_1064, delr, userTemp, i)

% These are defined as the values for the LIDAR ratios and the

S_a532 = [47];
S_a1064 = [33];
C = [1.2e+006];
C_1 = [330000];
start = 1;
finish = size(data_532, 1);

[beta_532 beta_1064 sigma_532 sigma_1064] = ...
    betaSigmaCalcNewer(data_532, data_1064, S_a532(i), S_a1064(i), start, ...
    finish, delr, userTemp, C, C_1);
```

Analysis Algorithms

General Calculations

```
function [data_532 data_1064 delr] = manipulation(data_532, data_1064, rbins)

% The PMT takes negative voltages so those need to be inverted.
data_532 = -data_532;

% The logical indexing gets rid of values that show negative return.
data_532(data_532 < 0) = 0;
data_1064(data_1064 < 0) = 0;

% This takes into account the responsivity of the detectors and the A-D
% conversion that takes place.

data_532 = (data_532/(2^14))*(3.9532e-005)*0.8;
data_1064 = (data_1064/(2^14))*(1.04165e-005)*1.15;

size_532 = size(data_532, 2);
size_1064 = size(data_1064, 2);

% The convolution further smooths the data.

h = ones(1)/1;
h1 = ones(1,7)/7;
```

```
data_532 = conv2(h',h1',data_532(:,1:size_532));
data_1064 = conv2(h',h1',data_1064(:,1:size(data_1064,2)));

% Redefinition of the zero using a region far out and assuming no return
% from it.

size_532 = size(data_532, 2);
size_1064 = size(data_1064, 2);

data_532a = data_532 - (mean(data_532(:,size_532 - 60:size_532 - 6), ...
2))*ones(1,size_532);
data_1064a = data_1064 - (mean(data_1064(:,size_1064 - 1000:size_1064 - ...
100),2))*ones(1,size_1064);

% The for loop normalizes the return to r^2

delr = rbins * 0.75;

for n = 7:size_532
    data_532(:,n) = data_532a(:,n)*(((n - 6)*delr)^2);
    data_1064(:,n) = data_1064a(:,n)*(((n - 6)*delr)^2);
end
clear data_532a data_1064a
```

Backscatter and Extinction Calculations

```
% This function will calculate the backscatter and extinction for both of
% the wavelengths.

function [beta_532 beta_1064 sigma_532 sigma_1064] = ...
    betaSigmaCalcNewer(data_532, data_1064, S_a532, S_a1064, start, ...
    stop, delr, userTemp, C, C_1)

% data_532 is the range corrected return at 532 nm
% data 1064 is the range corrected return at 1064 nm
% delr to be used in ranging and numerical integration.

% C is the 532 Calibration constant.
% C_1 is the 1064 Calibration constant. I still need to find this again.

r_0 = floor(500 / (delr / 0.75) );

% height is the height and it allows the temperature and pressure to be
% found as a function of altitude

len = size(data_532, 2);
hei = size(data_532, 1);
n = 1:len;
height = n*delr;
```

```
% Altitude adjusted tepurature

temp = userTemp - (0.006545 .* height);

% Altitude adjusted pressure

pressure = ( (288.15 ./ temp).^(-0.034164 / 0.006545) ).*(1.013e5);

q = length(S_a532);
beta_532 = zeros(hei,len,q);
beta_1064 = zeros(hei,len,q);
sigma_532 = beta_532;
sigma_1064 = beta_1064;


% Molecular backscatter
beta_M = (374.28 .* (pressure ./ temp) ./ (532^4) );

% Molecular constants
S_M = 8*pi/3;

% Molecular extinction
sigma_M = (beta_M * S_M);

% Transmittance for 532 as a function of height
T2 = height;
```

```
for i = 1:length(height)
    T2(i) = exp(-2*sum(sigma_M(1:i)));
end

% Molecular backscatter as a function of distance
int_func = zeros(1,len);

for n = 1:len
    int_func(n) = sum(beta_M(1:n) )*delr;
end

% backscatter at 532nm

for n = r_0:len
    beta_532(start:stop,n) = (data_532(start:stop,n) .* ...
        exp(-2 .* (S_a532 .* (sum(beta_M(r_0:n) ) .* ...
        delr) ) ) ./ ( (C .* (T2(r_0) ) ) - (2 * S_a532 .* ...
        (sum( (data_532(start:stop,r_0:n) ./ T2(n) ) .* ...
        exp(-2 .* (S_a532) * int_func(n) ), 2) * delr) ) ) - ...
        beta_M(n);
end

sigma_532(:,:) = beta_532(:,:) .* S_a532;
```

```
for n = r_0:len
    beta_1064(start:stop,n) = (data_1064(start:stop,n) ) ./ ...
        ( (C_1) - (2.* S_a1064 .* ...
        (sum(data_1064(start:stop,1:n) .* delr, 2) ) ) );
end


sigma_1064(:,:) = beta_1064(:,:) .* S_a1064;
```

APPENDIX B

LIST OF ACRONYMS

- LIDAR - LIght Detection And Ranging
- NASA - National Aeronautics and Space Administration
- AERONET - AErosol RObotic NETwork
- DIAL - DIfferential Absorption Lidar
- CCN - Cloud Condensation Nuclei
- CRAM - Constrained Ration Aerosol Model-fit
- Nd:YAG - Neodymium: Yttrium Aluminum Garnet
- APD - Avalanche Photo Diode
- PRF - Pulse Repetition Frequency
- FWHM - Full Width Half Maximum
- PMT - Photo Multiplier Tube
- D-H-V - Diagonal-Horizontal-Vertical
- CMOS - Complementary Metal-Oxide-Semiconductor
- A/D - Analog to Digital
- AOD - Aerosol Optical Depth
- MDT - Mountain Daylight Time
- HSRL - High Spectral Resolution Lidar
- FAA - Federal Aviation Administration